



**Michigan  
Technological  
University**

Michigan Technological University  
**Digital Commons @ Michigan Tech**

---

Dissertations, Master's Theses and Master's Reports

---

2018

## **PROBABILISTIC REGIONAL LANDSLIDE HAZARD ASSESSMENT FOR THE ENGURI DAM (JIVARI, GEORGIA)**

MARIA DILETTA ACCIARO

*Michigan Technological University, mdacciar@mtu.edu*

Copyright 2018 MARIA DILETTA ACCIARO

---

### **Recommended Citation**

ACCIARO, MARIA DILETTA, "PROBABILISTIC REGIONAL LANDSLIDE HAZARD ASSESSMENT FOR THE ENGURI DAM (JIVARI, GEORGIA)", Open Access Master's Thesis, Michigan Technological University, 2018. <https://digitalcommons.mtu.edu/etdr/640>

Follow this and additional works at: <https://digitalcommons.mtu.edu/etdr>



Part of the [Geological Engineering Commons](#), [Geotechnical Engineering Commons](#), and the [Risk Analysis Commons](#)

PROBABILISTIC REGIONAL LANDSLIDE HAZARD ASSESSMENT FOR THE  
ENGURI DAM (JVARI, GEORGIA)

By

Maria Diletta Acciaro

A THESIS

Submitted in partial fulfillment of the requirements for the degree of

MASTER OF SCIENCE

In Geology

MICHIGAN TECHNOLOGICAL UNIVERSITY

2018

© 2018 M. D. Acciaro

This thesis has been approved in partial fulfillment of the requirements for the Degree of MASTER OF SCIENCE in Geology.

Department of Geological and Mining Engineering and Sciences

Thesis Co-Advisor: *Thomas Oommen*

Thesis Co-Advisor: *John S. Gierke*

Committee Member: *Luke J. Bowman*

Department Chair: *John S. Gierke*

# Table of Contents

1	Introduction .....	1
2	Background .....	3
2.1	Project purpose and description.....	3
2.2	Objective of the study .....	4
2.3	Study area.....	4
2.4	Geology and Lithotypes .....	6
2.4.1	Caucasus Orogeny .....	6
2.4.2	Geology of Enguri dam area .....	10
3	Methodologies .....	13
3.1	Previous data collection and processing .....	13
3.1.1	Structural data from Tbilisi University.....	13
3.1.2	USGS ASTER Global DEM .....	14
3.1.3	GPS positions of the sliding zone.....	16
3.2	Field Investigation .....	17
3.2.1	Fieldwork on rocks .....	21
3.2.2	Fieldwork on soils.....	32
3.3	Landslides analysis .....	39
3.4	PISA-m.....	43
3.4.1	Digital Elevation Model.....	44
3.4.2	Lithologies.....	45
3.4.3	Normalized Difference Vegetation Index .....	46
3.4.4	PISA-m: Map Based Probabilistic Slope Analysis.....	48
3.4.5	Results.....	58
3.5	2D FEM-SSR Modeling.....	59
4	Results .....	73
5	Reference List and Copyright documentation.....	74

## List of Figures

Figure 1: Enguri dam looking north (source: [https://en.wikipedia.org/wiki/Enguri\\_Dam](https://en.wikipedia.org/wiki/Enguri_Dam))

Figure 2: Enguri dam geo localization on Google Maps (Abkhazia region on the left of the dashed line)

Figure 3: Enguri dam view from Google Earth (Abkhazia region on the left of the dashed line)

Figure 4: Geology of the Caucasus and adjacent areas: 1:2.500.000 scale geological map (Adamia et al., 2010)

Figure 5: Tectonic map of the Arabia - Eurasia collision zone (modified from Sosson et al., 2010). Abbreviations: GC-Greater Caucasus; LC-Lesser Caucasus; AT-Achara-Trialeti; R- Rioni; Dz-Dzirula; K-Kura; MB-Mus Basin; EP-Eastern Pontides; KM-Kirsehir Massif; EAF- Eastern Anatolian Fault; NAF-North Anatolian Fault; IAES-Izmir-Ankara-Erzincan Suture; MM-Menderes Massif (N. Tsereteli, et al., 2016)

Figure 6: Simplified tectonic map of the Caucasus (Modified from Adamia et al., 2011a, 2011b; Mosar et al., 2010). Abbreviations: RFFTB-Rioni foreland fold and thrust belt; RF-Rioni foreland; KFFTB-Kura foreland fold and thrust belt; KF-Kura foreland; ATFTB-Achara-Trialeti fold and thrust belt; BGKFTB-Baiburt-Garabagh-Kaphan fold and thrust belt; TFTB-Talysh fold and thrust belt; DZ-Dzirula; Kh-Khrami; Lo-Loki; Ts-Tsakhkuniats; K-Kazbegi. (Tsereteli, et al., 2016)

Figure 7: Geology of Caucasus, a review, Adamia et al.,2010

Figure 8: Geological map of the studied area (Adamia and Gujabadze, 2004)

Figure 9: Main tectonic elements, locations map and geological section (C. J. Banks et al., chapter 17)

Figure 10: Complete view of the arcMap shapefiles from Tibillisi University

Figure 11: Zoom of the study area on arcMap showing the lithology layer and some geomorphological structures (data from M.Nodia Institute of Geophysics)

Figure 12: Aspect and Slope map of the area from arcMap 10.3.1. Realized from M.D. Acciario, Scale 1:50.000

Figure 13: 1:40.000 scaled map of the GPS positions of the landslides area surveyed from J.S. Gierke on field

Figure 14: Fallen rocks at the border of the principal road

Figure 15: Example of a weak limestone outcrop

Figure 16: Road subsidence, evidence of Khoko landslide (1)

Figure 17: Road subsidence, evidence of Khoko landslide (2)

Figure 18: Map showing the GPS locations of the survey sites

Figure 19: Schmidt hammer calibration chart

Figure 20: Schmidt hammer calibration chart instructions

Figure 21: Point Load Test device from Michigan Technological University, department of Geological & Mining Engineering & Science

Figure 22: Geomorphological overview from Active inversion tectonics, simple shear folding and back-thrusting at Rioni Basin, Georgia. Tibaldi et al., 2016

Figure 23: Neogene-Paleogene surveyed outcrop (picture from F.L. Bonali)

Figure 24: Folded and fractured Cretaceous outcrop adjacent to the principal road

Figure 25: Detail of a Cretaceous outcrop

Figure 26: Upper Jurassic outcrop adjacent to the principal road

Figure 27: Detail of an Upper Jurassic outcrop

Figure 28: Middle Jurassic outcrop adjacent to the principal road

Figure 29: Detail of a Middle Jurassic outcrop

Figure 30: Clay mass over the sliding area characterized by gypsum inclusions

Figure 31: Gypsum quarry in the Upper Jurassic unit, over the south Khoko niche

Figure 32: Detail of an Upper Jurassic loose outcrop

Figure 33: Cone Penetration Test (CPT) device on the left and Shear Vane device on the right. Machines from the Geological & Mining Engineering & Science department of the Michigan Technological University

Figure 34: Press used for the calibration of the CPT device, laboratory of geotechnics of the Geological & Mining Engineering & Science department of the Michigan Technological University

Figure 35: Excel file screenshot of the values used for the calibration of the CPT device

Figure 36: Basic classification of landslides: 1.Fall, 2.Topple, 3.Slide, 4.Spread, 5.Flow (Cruden and Varnes, 1996)

Figure 37: Detachment niches of Khoko landslide (south) and of a hypothetical bigger structure (north)

Figure 38: Drainage basin of the area. Light blue: flow pattern; dark blue: watershed

Figure 39: Smaller bodies and swollen areas identified over the hypothetic landslide

Figure 40: Fractures and general morphological discontinuities

Figure 41: Faults

Figure 42: DEM arcMap map

Figure 43: Lithologies arcMap map

Figure 44: NDVI arcMap map

Figure 45 Factor of safety FS formula for a forested infinite slope (source: PISA-m manual, William C. Haneberg)

Figure 46: Command prompt example to run PISA-m

Figure 47: Parameter file (.par) example (source: PISA-m manual, William C. Haneberg)

Figure 48: Entries to implement the different calculations on PISA-m (source: PISA-m manual, William C. Haneberg)

Figure 49: PISA-m results. Spatial distribution of the safety factor around the area for different values of friction ( $\Phi$ ). a) $\Phi=0$  b) $\Phi=10$  c) $\Phi=30$

Figure 50: 2D section of the slope on Phase2 (Total Head 510m)

Figure 51: Maximum Shear Plastic Strain MODEL2

Figure 52: Total Displacement MODEL2

Figure 53: Solid Horizontal Displacement MODEL2

Figure 54: Solid Vertical Displacement MODEL2

Figure 55: Phase2 MODEL2.A

Figure 56: Phase2 MODEL2.B

Figure 57: Shear Plastic Strength MODEL 2.A

Figure 58: Shear Plastic Strength MODEL 2.B

Figure 59: Solid Vertical Displacement MODEL 2.A

Figure 60: Solid Vertical Displacement MODEL 2.B

Figure 61: Solid Horizontal Displacement MODEL 2.A

Figure 62: Solid Horizontal Displacement MODEL 2.B

Figure 63: Yielded Elements MODEL 2.A

Figure 64: Yielded Elements MODEL 2.B

Figure 65: Maximum Shear Plastic Strain and deformation vectors MODEL 2.A

Figure 66: Maximum Shear Plastic Strain and deformation vectors zoom MODEL2.A

Figure 67: Maximum Shear Plastic Strain and deformation vectors MODEL2.A.430

Figure 68: Maximum Shear Plastic Strain and deformation vectors zoom  
MODEL2.A.430

Figure 69: Slide MODEL2.A (FS for Janbu Simplified)

Figure 70: Slide MODEL2.A.430 (FS for Janbu Simplified)



## List of Tables

**Table 1**

Moist unit weight	Middle Jurassic	Upper Jurassic rocks	Upper Jurassic soils	Cretaceous	Neogene
Gm	26.01	27.46	21.48	27.46	25.01
kN\m3	26.12	26.97	20.59	28.44	25.12
	26.25	25.79	24.03	22.55	25.25
	26.34	22.75	22.84	23.53	25.34
	26.45	22.06	19.03	24.52	25.45
	26.7	28.27	18.54	25.89	25.56
	27.3	25.3	19.12	26.5	25.7
	27.5	20.01	19.61	24.71	26.22
<b>average</b>	26.5838	24.8263	20.6550	25.4500	25.4563
<b>st. dev</b>	0.5476	2.9205	1.9789	1.9923	0.3821
<b>min</b>	26.01	20.01	18.54	22.55	25.01
<b>max</b>	27.5	28.27	24.03	28.44	26.22

**Table 2**

Saturated Unit weight	<b>Middle Jurassic</b>	<b>Upper Jurassic rocks</b>	<b>Upper Jurassic soils</b>	<b>Cretaceous</b>	<b>Neogene</b>
Gs	27.01	29.46	22.48	28.46	26.01
kN\m3	27.12	28.97	22.59	30.44	26.12
	27.25	26.79	26.03	24.55	26.25
	27.34	24.75	24.84	25.53	26.34
	27.45	24.06	21.03	27.52	26.45
	27.7	30.27	20.54	26.89	26.56
	28.3	27.3	21.12	28.5	26.7
	28.5	22.01	21.61	25.71	27.22
<b>average</b>	27.5838	26.7013	22.5300	27.200	26.4563
<b>st. dev</b>	0.5476	2.8946	1.9507	1.9274	0.3821
<b>min</b>	27.01	22.01	20.54	24.55	26.01
<b>max</b>	28.5	30.27	26.03	30.44	27.22

**Table 3**

Unit weights of the lithologies					
Moist unit weight Gm kN\m <sup>3</sup>	<b>Middle Jurassic</b>	<b>Upper Jurassic rocks</b>	<b>Upper Jurassic soils</b>	<b>Cretaceous</b>	<b>Neogene</b>
<b>average</b>	26.5838	24.8263	20.6550	25.4500	25.4563
<b>st. dev</b>	0.5476	2.9205	1.9789	1.9923	0.3821
<b>min</b>	26.01	20.01	18.54	22.55	25.01
<b>max</b>	27.5	28.27	24.03	28.44	26.22
Saturated Unit weight Gs kN\m <sup>3</sup>	<b>Middle Jurassic</b>	<b>Upper Jurassic rocks</b>	<b>Upper Jurassic soils</b>	<b>Cretaceous</b>	<b>Neogene</b>
<b>average</b>	27.5838	26.7013	22.5300	27.200	26.4563
<b>st. dev</b>	0.5476	2.8946	1.9507	1.9274	0.3821
<b>min</b>	27.01	22.01	20.54	24.55	26.01
<b>max</b>	28.5	30.27	26.03	30.44	27.22

**Table 4**

Rock mass survey, GPS locations							
<b>Cretaceous</b>	<b>family</b>	<b>orient</b>	<b>fill</b>	<b>R</b>	<b>angle</b>	<b>Point Load</b>	<b>GSI</b>
<b>K</b>	1	295\32	silt	30,31,31,20	501	42,8	25 35
						34,4	
	2	190\63	silt	41,42,43	503	34,4	
	3	102\86	silt	32	503	40,6	
	1	250\90	silt	27	505	33,6	
	4	6\37	silt	10,11,15	501	58,8	
	5 wall	154\63		30,35,28,5,5,5,5,24,29,55,20,35,44,25,44,20	505		
<b>J</b>	wall		silt	18,5,26,40,30,15	505		
<b>L</b>	1	295\85	no	5,5,29,16,30,17,35,22,19	505	44,8	40 35
						45,7	
	4wall	15\80		14,54,50,44,29,55,20	505	54,6	
	2	290\89	sand	55,10,35,5,11,11,	503	34,6	

				19			
	3	12\39	silt	26,47,11, 10,35,40, 45	501		
<b>M</b>	1	112\68	clay\ silt	25,21,22	505	60	45
						38,6	
	2	295\65	no	44	503	10,6	
	3	120\64	no	52,50,59	503		
	4	154\38	calci te	44,40	507		
	5 wall	30\70	no	29,12,44, 24,50,32, 26,5,25	505		
<b>N</b>	1	350\5	no	30,48,30	503,5 03,50 7	13	25 30
						60	
	2wall	49\82	no	26,52,42, 10	505	30	
	3	157\60	no	5,18,32, 28	507		
<b>Neogene</b>	<b>family</b>	<b>orient</b>	<b>fill</b>	<b>R</b>	<b>angle</b>	<b>Point Load</b>	<b>GSI</b>
	no	massive		11,20,41, 30,23,25, 46,22,26,	505	25,45	60

				35,24,22, 20,22,32, 36,21,16, 46,21,38			
<b>Upper Jurassic</b>	<b>family</b>	<b>orient</b>	<b>fill</b>	<b>R</b>	<b>angle</b>	<b>Pnt.Load</b>	<b>GSI</b>
<b>O</b>	wall	90\68	no	31,42,37, 43,44,16, 32,28,43, 22	505, 503	52,2 16,6	55 45
<b>P</b>	wall		no	36,34,54, 47,51,63, 61,62,45, 34,48,22, 32	505,5 01	35 38,2 22 14,2 12 13	55
<b>Q</b>	1/		no	47	503		55
	2\		no	28	507		65
	3		no	60	505		
<b>R</b>	wall		no	30	505		55
			no	44,16	505		65
<b>Middle Jurassic</b>	<b>family</b>	<b>orient</b>	<b>fill</b>	<b>R</b>	<b>angle</b>	<b>Point Load</b>	<b>GSI</b>
<b>U</b>	1	300\60	no	40,36,46,	507,	\	70

				44,26,22	503		
	2	157\51	no	39,34,36, 48,16,52	507		
	3 vert		no	\			
	4 wall	245\76	no	20,43,52, 51,44,22, 27	505		
	5 horz	255\33	no	52,27	509		
<b>V</b>	1	65\75	no	39,37,32	505	\	70
	2	258\42	no	66	503		
	3 horz	175\55	no	18,40,26	501		
	4	222\47	no	64,62,60, 55,46,36	507		
	5 wall	144\64	no	38,36,44, 30,35	505		

**Table 5**

Schmidt Hammer test results (average of values)			
<b>Neogene</b>	<b>Cretaceous</b>	<b>Upper Jurassic</b>	<b>Middle Jurassic</b>
<b>UCS- R505</b>	<b>UCS- R505</b>	<b>UCS- R505</b>	<b>UCS- R505</b>
38.74097 MPa	42.6204 MPa	57.7186 MPa	92.3844 MPa
	<b>UCS- R507</b>	<b>UCS- R501</b>	
	28.7031 MPa	42.7682 MPa	
	<b>UCS- R503</b>	<b>UCS- R503</b>	
	40.0883 MPa	42.7350 MPa	
	<b>UCS- R501</b>	<b>UCS- R507</b>	
	42.4186 MPa	32.0372 MPa	



**Table 6**

Point Load Test on field (K=24)								
Cretaceous			Jurassic			Neogene		
Is50 (bar)	Is50 (Mpa)	UCS= K*Is50	Is50 (bar)	Is50 (Mpa)	UCS= K*Is50	Is50 (bar)	Is50 (Mpa)	UCS= K*Is50
42.8	4.28	102.72	52.2	5.22	125.28	25.45	2.545	61.08
34.4	3.44	82.56	16.6	1.66	39.84			
34.4	3.44	82.56	35	3.5	84			
40.6	4.06	97.44	38.2	3.82	91.68			
33.6	3.36	80.64	22	2.2	52.8			
58.8	5.88	141.12	14.2	1.42	34.08			
44.8	4.48	107.52	12	1.2	28.8			
45.7	4.57	109.68	13	1.3	31.2			
54.6	5.46	131.04						
34.6	3.46	83.04						
60	6	144						
38.6	3.86	92.64						
10.6	1.06	25.44						

13	1.3	31.2						
60	6	144						
30	3	72						

**Table 7**

<b>STRENGTH OF ROCKS</b>	Neogene	Cretaceous	Upper Jurassic	Middle Jurassic
UCS from Schmidt Hammer on discontinuities surfaces	38740,97 kPa	38457,6 kPa	43814,75 kPa	92384,4 kPa
UCS from Point Load Test on samples	61080 kPa	95475 kPa	60960 kPa	-
GSI	60	34	56	70

**Table 8**

CPT test (x=pounds;y=inches) on the Upper Jurassic soils								
Inches (CPT)	lb. linear at (0.0) =Qc	GPS	ov	Nk	qc=(Qc/Ac ) Ac=1 in <sup>2</sup>	Su (psi)	φ	c (MPa) =Su
0.02505	38.45011307	BH8 .1	0	9.6	38.4501131	4.00522	0	0.027615
0.01145	16.72959229		0	9.6	16.7295923	1.742666	0	0.0120153
0.0241	36.93287081		0	9.6	36.9328708	3.847174	0	0.0265253
0.11755	186.1815963	BH8 .2	0	9.6	186.181596	19.39392	0	0.1337164
0.1226	194.2469368		0	9.6	194.246937	20.23406	0	0.1395089
0.0946	149.5282175	Min e area	0	9.6	149.528218	15.57586	0	0.1073918
0.12505	198.1598247	Min e	0	9.6	198.159825	20.64165	0	0.1423192
0.1151	182.2687084		0	9.6	182.268708	18.98632	0	0.1309061
0.07715	121.6588728		0	9.6	121.658873	12.6728	0	0.0873759

0.1128	178.595385		0	9.6	178.595385	18.60369	0	0.1282679
0.099	156.5554448		0	9.6	156.555445	16.30786	0	0.1124388
0.09745	154.0799443	B	0	9.6	154.079944	16.04999	0	0.1106608
0.1058	167.4157052		0	9.6	167.415705	17.43914	0	0.1202386
0.1136	179.8730627		0	9.6	179.873063	18.73678	0	0.1291856
0.10025	158.5518162		0	9.6	158.551816	16.51581	0	0.1138726
0.0815	128.6062453	BH3	0	9.6	128.606245	13.39648	0	0.0923655
0.10215	161.5863007		0	9.6	161.586301	16.83191	0	0.1160519
0.0844	133.2378269		0	9.6	133.237827	13.87894	0	0.0956919
0.1021	161.5064459		0	9.6	161.506446	16.82359	0	0.1159946
0.0756	119.1833723	T	0	9.6	119.183372	12.41493	0	0.085598
0.0869	137.2305697		0	9.6	137.23057	14.29485	0	0.0985596

0.08785	138.747812		0	9.6	138.74781 2	14.4529	0	0.0996492
0.05155	80.77318666		0	9.6	80.773186 7	8.41387 4	0	0.0580116

**Table 9**

Shear Vane Test ( $\Phi=0$ ) on the Upper Jurassic soils					
Shear Vane ( $^{\circ}$ )	GPS	T (ft-lbs)	D (ft)	Su (psf)	Su (MPa)= c
46	BH8.1	0.2829	0.0625	316.1829	0.0151
39		0.2253	0.0625	251.819	0.0121
115		0.8506	0.0625	950.6267	0.0455
55	BH8.2	0.3570	0.0625	398.9364	0.0191
60		0.3981	0.0625	444.9106	0.0213
82		0.5791	0.0625	647.197	0.0310
75		0.5215	0.0625	582.8332	0.0279
155	BH8	1.1798	0.0625	1318.42	0.0631
120		0.8918	0.0625	996.6008	0.0477
120		0.8918	0.0625	996.6008	0.0477
96	Mine Area	0.6943	0.0625	775.9247	0.0372
56		0.3652	0.0625	408.1312	0.0195
59		0.3899	0.0625	435.7158	0.0209

70		0.4804	0.0625	536.859	0.0257
65		0.4393	0.0625	490.8848	0.0235
90	Mine	0.6449	0.0625	720.7557	0.0345
44		0.2665	0.0625	297.7932	0.0143
82		0.5791	0.0625	647.197	0.0310
83		0.5874	0.0625	656.3919	0.0314
84		0.5956	0.0625	665.5867	0.0319
85		0.6038	0.0625	674.7815	0.0323
73		0.5051	0.0625	564.4435	0.0270
114	B	0.8424	0.0625	941.4318	0.0451
116		0.8589	0.0625	959.8215	0.0460
74		0.5133	0.0625	573.6383	0.0275
109		0.8013	0.0625	895.4576	0.0429
114		0.8424	0.0625	941.4318	0.0451
141		1.0646	0.0625	1189.692	0.0570
140		1.0563	0.0625	1180.498	0.0565



112		0.8260	0.0625	923.0421	0.0442
137		1.0317	0.0625	1152.913	0.0552
48	BH3	0.2994	0.0625	334.5725	0.0160
40		0.2336	0.0625	261.0138	0.0125
38		0.2171	0.0625	242.6242	0.0116
114		0.8424	0.0625	941.4318	0.0451
75		0.5215	0.0625	582.8332	0.0279
55		0.3570	0.0625	398.9364	0.0191
51		0.3241	0.0625	362.1571	0.0173
44		0.2665	0.0625	297.7932	0.0143
48	T	0.2994	0.0625	334.5725	0.0160
86		0.6120	0.0625	683.9764	0.0327
57		0.3734	0.0625	417.3261	0.0200
50		0.3158	0.0625	352.9622	0.0169
164	trench	0.0625	1.2538	1401.174	0.06709
228	"	0.0625	1.7804	1989.643	0.09526

312	"	0.0625	2.4715	2762.01	0.13225
350	"	0.0625	2.7842	3111.413	0.14898
254	"	0.0625	1.9943	2228.709	0.10671
341	"	0.0625	2.7101	3028.66	0.14501
274	"	0.0625	2.1589	2412.606	0.11552
238	"	0.0625	1.8627	2081.592	0.09967
351	"	0.0625	2.7924	3120.608	0.14942
299	"	0.0625	2.3645	2642.477	0.12652

**Table 10**

	Neogene		Cretaceous		Upper Jurassic soils		Upper Jurassic rocks		Middle Jurassic	
	c	$\Phi$	c	$\Phi$	c	$\Phi$	c	$\Phi$	c	$\Phi$
<b>avrg.</b>	0.2850	42.2750	0.2150	35.0100	0.0116	30	0.4600	50.2070	0.6470	55.1780
<b>st.dev</b>	0.5160	53.4840	0.5940	52.5290	0.1423	0	1.8580	64.9740	2.2040	66.0500
<b>max</b>	0.3809	47.6762	0.3537	43.3712	0.0547	30	0.9061	57.9476	1.2564	61.2994
<b>min</b>	0.0652	3.0812	0.1045	5.1578	0.0407	30	0.3734	4.1923	0.4882	3.3999

**Table 11.1**

a) Physical parameters required on PISA-m (average±standard deviation)					
<b>Neogene</b>	<b>Cretaceous</b>	<b>Upper Jurassic soils</b>	<b>Upper Jurassic rocks</b>	<b>Middle Jurassic</b>	<b>Parameters</b>
48 (±3)	43 (±5)	30 (±)	58 (±4)	61 (±3)	<b>Friction Angle (°)</b>
380 (±65)	350 (±100)	63 (±44)	910 (±370)	1260 (±490)	<b>Cohesive Strength (kPa)</b>
26,5 (±0.4)	27,2 (±2)	22,5 (±2)	26,7 (±3)	27,6 (±0.5)	<b>Saturated Unit Weight (kN\m<sup>3</sup>)</b>
25,5 (±0.4)	25,5 (±2)	20,7 (±2)	24,8 (±3)	26,6 (±0.5)	<b>Moist Unit Weight (kN\m<sup>3</sup>)</b>

**Table 11.2**

b) Physical parameters required on PISA-m		
<b>Gw (Pa)</b>	<b>min_Slope (°)</b>	<b>z_err</b>
9810.0	5	10

**Table 12.1**

a) Physical Parameters legend	
gw	Unit weight of water (kN\m <sup>3</sup> )
an	User-specified Newmark acceleration threshold (g)
dn	User-specified Newmark displacement (cm)
IA	Arias intensity of the earthquake for Newmark displacement calculations (m\s)
minslope	Minimum slope angle (degrees)
z_err	DEM elevation error standard deviation (units consistent with the DEM)

**Table 12.2**

b) Physical parameters legend	
phi	Angle of internal friction (degrees)
cs	Soil cohesive strength (pressure)
d	Soil thickness (length)
h	Pore pressure coefficient ( $0 \leq h \leq 1$ )
gs	Saturated unit weight (force\volume)
gm	Moist unit weight (force\volume)

**Table 13**

Parameters of the lithologies implemented in the example.par
soils 7
phi normal 58 4.19 0
cs normal 906 373.41 0
d uniform 10 20 0
h uniform 0.1 0.5 0
gs normal 26701 2894.62 0
gm normal 24826 2920.47 0

phi normal 48 3.08 0

cs normal 381 65.20 0

d uniform 2 10 0

h uniform 0.1 0.5 0

gs normal 26456 382.06 0

gm normal 25456 382.06 0

phi normal 40 0. 0

cs normal 55 40.71 0

d uniform 10 20 0

h uniform 0.1 0.5 0

gs normal 22530 1950.71 0

gm normal 20655 1978.88 0

phi normal 48 3.08 0

cs normal 381 65.20 0

d uniform 2 10 0

h uniform 0.1 0.5 0

gs normal 26456 382.06 0

gm normal 25456 382.06 0

phi normal 61 3.40 0

cs normal 1256 488.17 0

d uniform 10 15 0

h uniform 0.1 0.5 0

gs normal 27584 547.59 0

gm normal 26584 547.59 0

phi normal 40 0. 0

cs normal 55 40.71 0

d uniform 10 20 0

h uniform 0.1 0.5 0

gs normal 22530 1950.71 0

gm normal 20655 1978.88 0

phi normal 43 5.16 0

cs normal 354 104.53 0

d uniform 10 20 0

h uniform 0.1 0.5 0

gs normal 27200 1927.44 0

gm normal 25450 1992.31 0



**Table 14**

	<b>Φ (°)</b>	<b>c (Kpa)</b>	<b>Y (kN/m<sup>2</sup>)</b>	<b>E (kPa)</b>	<b>PTS (kPa)</b>	<b>RTS (kPa)</b>	<b>v</b>
CLAY	20	50	19.55	100,000	20	0	0.3
WB	32	100	22	10,000,000	50	0	0.3
IB	35	200	25	10,000,000	100	0	0.3

**Table 15**

	$\Phi$ (°)	c (Kpa)	Y (kN/m <sup>2</sup> )	E (kPa)	PTS (kPa)	RTS(kPa)	v
<b>CLAY</b>	20	50	19.55	100,000	20	0	0.3
<b>WB</b>	32	100	22	10,000,000	50	0	0.3
<b>IB</b>	35	200	25	10,000,000	100	0	0.3
<b>STABLE</b>	50	500	27	10,000,000	100	0	0.3

## Acknowledgements

I would first like to thank my advisors Dr. John S. Gierke, Dr. Thomas Oommen and Dr. Luke Bowman of the department of Geological Engineering and Sciences of Michigan Technological University and Dr. Federico Agliardi and Alessandro Tibaldi of the Dipartimento di Scienze e Tecnologie Geologiche of Milano Bicocca University. Their door was always open whenever I ran into a trouble spot or had a question about my research and my writing. No matter the commitments and the distances, they consistently allowed this research to grow, helping me and enduring my thousand emails. They steered me in the right direction whenever I needed it. Thanks also to both the universities office staff Kelly McLean, Brittany Buschell, and Angela Sanna that helped me with the hard process of the documentation. Thanks to Kiko Silvelet and Stanley Vitton for their fundamental help before the field trip, they provided me valid instrumentation and explanations. I would especially like to thank the Georgian experts who were involved in my same research project. They helped me all the time, sharing their knowledges and inspiring me: Nino Tserteli, Davit Odilavadze, Victor Alania, Onise Enuquidze, Nino Kvavadze, Aleksndre Gventsadze. Thanks to them, to Paolo Oppizzi and especially John Gierke my work in Georgia was amazingly fun and intense and made me grow professionally, socially and culturally. My work could not have been successfully conducted without their passionate participation, their input and their help. Finally, I must express my very profound gratitude to my parents, which love, support and tolerate me no matter how hard it can be. Nothing of what I did would have been possible without them. Thanks to them, to my relatives and my closest friends to provide me unfailing support and continuous encouragement throughout this last months. Everything I did in the last couple of years was a life experience more than just a research.

## Abstract

The Enguri Dam forms a reservoir in a seismically active area in the foothills of the Caucasus Mountain range near Jvari, Georgia. The slopes are steep, highly fractured, and weathered which make them at risk to failure during or following extreme rainfall events. Hydroelectricity produced by the water retained by the 271-m dam provides almost half of the electricity for the country. The reservoir perimeter is more than 40 km and the surrounding slopes span an area of more than 30 km<sup>2</sup>. The size of the area and paucity of slope data have made slope-failure hazard assessment of the broader area impossible. Only limited previous work has been completed and it was focused on a single creeping landslide. This work evaluated the landslide hazards for the reservoir area using data from past studies, field investigations, and remotely sensed inputs integrated with Geographic Information System (GIS) based slope stability analysis. The GIS-based Probabilistic Infinite Slope Analysis modeling (PISA-m) program was used to evaluate the static slope stability of the region. The geotechnical properties (e.g., unit weight, angle of internal friction, cohesive strength, and moisture content) were obtained from published literature and field data collection. The remotely sensed Normalized Difference Vegetation Index (NDVI) derived from Landsat 8 was used to account for the vegetation distributions in calculations of root strengths for the slopes. The uncertainties in the input parameters were estimated using extreme value distributions. The static and seismic slope stability analysis revealed that the areas proximal to the dam have minimal safety factors against sliding and are highly susceptible to slope instability, especially in seismic events. The verification of the modeled stability with the landslides mapped using high-resolution remotely sensed data and fieldwork indicates that the PISA-m provides a promising program for regional slope stability analysis. Furthermore, to better understand the mechanics of the sliding area, we performed a Finite Element slope stability analysis with Rocscience Phase2 and a Limit Equilibrium analysis with Rocscience Slide.

# 1 Introduction

This research is part of a North Atlantic Treaty Organization (NATO) Science for Peace and Security Programme. The project is titled “NATO Project G4934 – Science for Peace and Security Programme. Its purpose is to evaluate the vulnerability of the Enguri Dam to geohazards. The Enguri Dam (Figure 1) is the largest hydroelectric facility in the Republic of Georgia (Figure 2) and one of the highest concrete arch dams in the world with a maximum height of 271.5 m. Construction began in 1961 and was completed in 1987. Soviet President Nikita Khrushchev initially proposed to build the dam on the Bzyb River, which is the location of his favorite resort, however studies suggested that the dam would have had a catastrophic effect on the beach erosion at Pitsunda. Therefore, the dam was built on the Enguri River instead where there was no forecast of negative impacts on the coastline (Blatter and Ingram, 2001). The facility is part of the Enguri hydroelectric power station (HES) in a Transcaucasian area 5 km northwest of the city of Jvari and 2 km north of Potskho Etseri. The Transcaucasian area has 8000 inhabitants among hundreds of sparse rural settlements. The Enguri River is an approximate eastern boundary of the separatist region of Abkhazia (Figure 3) which is currently a post-independence conflict zone. Several conflicts occurred during the 1990s in the disputed territories and although the region has not experienced conflicts since, the situation is still not resolved. This NATO SPS project is supported by more than 30 academics from different institutions based in the United States, the European Union, and the Caucasus region. The project consists of complementary elements for assessing potential hazards to the dam, including: seismicity (earthquakes), landslides (rainfall and seismically induced), tsunami due to a catastrophic landslide, and flooding (<http://www.enguriproject.unimib.it/>).



Figure 1: Enguri Dam looking north (source: [https://en.wikipedia.org/wiki/Enguri\\_Dam](https://en.wikipedia.org/wiki/Enguri_Dam))

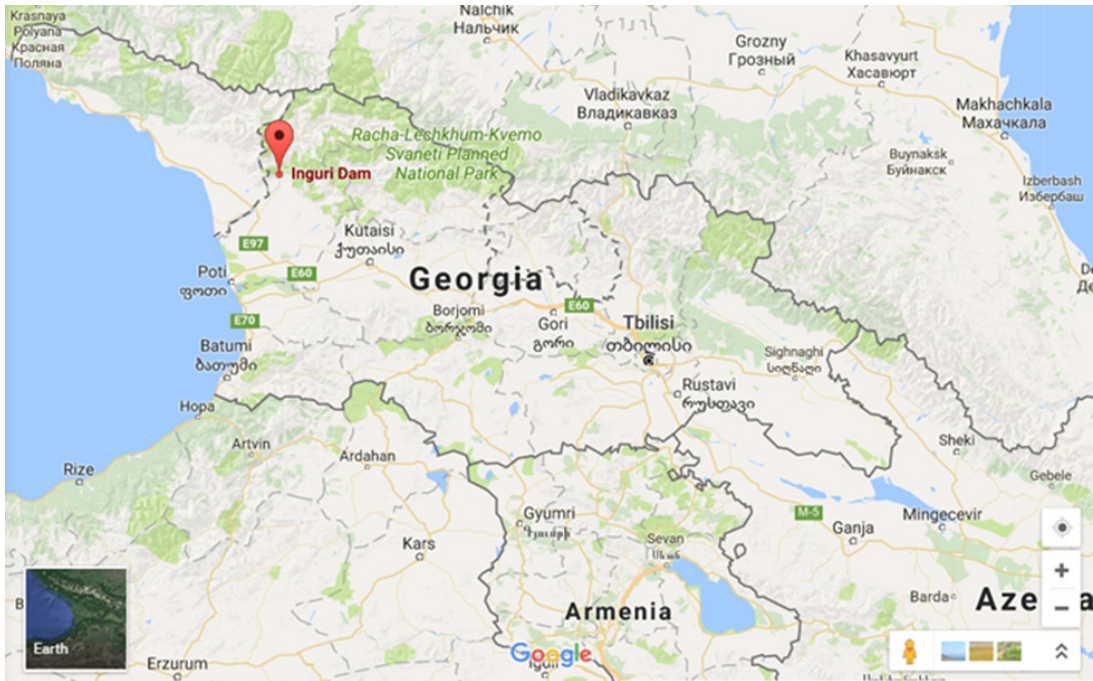


Figure 2: Enguri Dam geo localization on Google Maps (Abkhazia region on the left of the dashed line)



Figure 3: Enguri Dam view from Google Earth (Abkhazia region on the left of the dashed line)

## 2 Background

### 2.1 Project Purpose and Description

The SPS programme is a policy tool that fosters innovative scientific cooperation between different international partners with complementary expertise. NATO funding supports the research addressing important problems while helping to also build capacity for research through training and experience for young researchers and to improve the international knowledge exchange. These types of projects are generally developed by a (NATO) member in conjunction with partners that include both NATO and non-NATO countries. The nations involved in this work are Italy (NATO lead), Georgia (non-NATO lead), Switzerland, United Kingdom (UK), United States of America (USA), Kazakhstan, and Azerbaijan. The purpose of this research is to evaluate the vulnerability of Enguri Dam to geological hazards.

The dam is located in a Transcaucasian area, on the southern slope of the Caucasus Fold and Thrust Mountain Belt. The foothill is characterized by several active faults spanning from the belt to the Caspian Sea, increasing the potential for seismically triggered landslides. As the primary infrastructure that supplies approximately half of the energy needs for Georgia, a catastrophe that impacts its operation would have significant impacts on the Georgian economy and could destabilize the fragile geopolitical situation in the region. The worst scenario includes flooding induced by the spill of material in the dam's reservoir.

The duties of each research group are categorized in four principal objectives:

- local seismic hazard assessment;
- landslide hazard assessment;
- tsunami and flooding hazards assessment;
- data process, interpretation and dissemination of results using GIS.

The Georgian and the Italian groups together with the researchers from the UK and Azerbaijan, are working on the seismic hazard assessment by analyzing the area through geology, tectonic, and geophysical examination. The USA team, of which the author of this thesis is a member, was tasked with the landslide hazard assessment. We are using numerical modeling to create a landslide susceptibility map. The UK team is analyzing the tsunami hazard assessment, and the Kazakhstan and Italian teams are working on the dissemination and the sharing of results (Tibaldi and Mumladze, NATO SPS project plan report). The project website can be consulted at <http://www.enguriproject.unimib.it/>.

## 2.2 Objective of the Study

The principal goal of this thesis is to conduct a landslide susceptibility analysis of the area. The first step was the development of a map-based probabilistic stability analysis for the slopes surrounding the reservoir to create a susceptibility map for slope failure under static load and undrained conditions. Analyzing all the aspects of this nearly unexplored area, I estimated the factor of safety (FOS) against sliding, which is the ultimate goal of this thesis work. The following objectives were systematically achieved to accomplish this overarching goal:

- 1) Compile background information on the geology, topography, vegetation, seismicity, climate, and land use of the area.
- 2) Identify remote sensing imagery for developing model input.
- 3) Identify computational tools appropriate for the slopes surrounding the reservoir.
- 4) Conduct field work to measure mechanical properties of the surficial geology.
- 5) Develop appropriate model inputs to create slope stability maps and perform sensitivity analyses on model parameters that were important and uncertain.

The analysis was executed following different phases, realizing the geological and geotechnical investigation.

PISA-m (Haneberg 2004- 2005) was identified as an appropriate modeling tool that would provide spatial analysis of the slope stability based on factors of safety. The best estimates of the model parameters were used with PISA-m to create a base-case susceptibility map. From this I numerically studied the variability of the output (FOS values) in response to varying the following physical parameters: coefficient of internal friction, cohesion, vegetation coverage, and soil-water content. Afterwards we obtained the finite elements analysis for a specific by slope applying Rocscience Phase2 and Slide to study the shear strength reduction and the FS.

## 2.3 Study Area

Large and rapid mass movement of earthen materials can cause flooding and even tsunami-like events that can breach a dam. The Michigan Technological University project team, of which I was a member, analyzed landslide hazards by gathering information on the potentially hazardous areas and performed a slope stability analysis to create a stability model for the project area. The geological and geotechnical analysis of the slopes surrounding the reservoir is a fundamental requisite to create a susceptibility map. The landslide hazard level of the area is evidently high: historical data and field work indicates several small landslides occurred at the slopes near the reservoir. One of many indicative examples is a 400 m tall mass of sediment on the east of the reservoir,



the Khoko landslide (Tibaldi and Mumladze, NATO SPS project plan report) that is apparently sliding (creeping) toward the reservoir.

Generally, the induction or reactivation of landslides can be triggered in a variety of different ways:

- Weak and soluble lithotypes: the area analyzed is composed of weak Jurassic and Cretacic lithologies.
- Increase of water pressure: excess water (as infiltration and runoff) and pore pressure are generally the most common cause of landslides. The fluctuation of the groundwater level due to heavy rains can increase the water pressure and induce gravitational movement on the more vulnerable slopes. Significant data from the Enguri Hydroelectric power station construction report can give an idea of the hydrological situation of the dam's area as summarized below (Deloitte consulting for USAID, Hydropower Investment Promotion Project HIPP).
  - ✓ Total drainage for the Enguri upper river basin = 194.7 km<sup>2</sup>;
  - ✓ Maximum and minimum plant discharge = 12.8 m<sup>3</sup>/s and 0.3 m<sup>3</sup>/s;
  - ✓ Average annual flood = 31.5 m<sup>3</sup>/s;
  - ✓ Highest recorded flow = 107 m<sup>3</sup>/s;
  - ✓ Calculated 100-yr flood based on a record period of 14 years = 73 m<sup>3</sup>/s.
- Seasonal increase of sediment within the rivers due to glaciers activity: Enguri dam is located at the southern slope of the Great Caucasus, residence of many glaciers. Seasonal and long-term temperature changes can negatively affect the hydrologic inputs to watersheds and rivers, changing the discharge.
- Seismicity can cause catastrophic landslides or exacerbate slope instabilities already burdened by wet seasons and weak geological materials. High peak ground acceleration (PGA) potential exists because of the high seismic hazard due to orogenic processes. Active tectonic faults exist along all the Caucasus foothills. Tectonic structures are pervasive in the area around Enguri including, for example, the Tkvarcheli flexural fold (Abkhazia) and Ingirishi up thrust (adjacent to the dam wall). The PGA levels are medium to high. All data is available on the on-line Earthquake database of the USGS National Earthquake Information Center <http://earthquake.usgs.gov/earthquakes/eqarchives/epic/>.

In all of the Caucasus area there been recorded 451 acceleration time histories from 269 earthquakes (Smith et al., 2000).

- Steep slope gradients are the most prevalent characteristic of unstable slopes. A landslide is defined as "the movement of a mass of rock, debris, or earth down a slope" (Cruden, 1991). The slopes all around the Enguri Dam reservoir are very steep, fractured, and deformed.

## 2.4 Geology and Lithotypes

The Enguri area is among a relatively young mountain fold and thrust belt that is in a thriving orogenic phase referred to as the Caucasus (Figure 4).



Figure 4: Geology of the Caucasus and adjacent areas: 1:2.500.000 scale geological map (Adamia et al., 2010)

### 2.4.1 Caucasus Orogeny

The Caucasus mountain range is a NW-SE directed mountain range spanning more than 1100 km and forms part of the border between Europe and Asia, extending from the eastern part of the Crimean Peninsula, to the Black sea, and to the Caspian Sea (Figure 4). The region, oriented WNW-ESE, is a large, active collisional orogeny. The Caucasus mountain range is divided in two principal parts: the Greater Caucasus Range and the Lesser Caucasus range, divided from the Transcaucasian massif. The highest point of this

mountain system is Mount Elbrus, a dormant stratovolcano that was active during the Holocene and is 5642-m high. The Cenozoic collision between the Arabian and Eurasian plates caused the closing of previous intra-arc and back-arc basins accompanied by inversion tectonics (Figure 5). This produced the development of the double fold-and-thrust belts referred to as the Greater and Lesser Caucasus which are separated by the Black Sea, the Rioni basin, and the South Caspian-Kura intermontane depression (Adamia et al., 1977, 2010; Banks et al., 1997; Mosar et al., 2010; Sosson et al., 2010). The Enguri area we analyzed is bounded to the south by the Transcaucasian massif, a paleo island-arc, and to the north by the Scythian platform (Adamia et al. 2011).

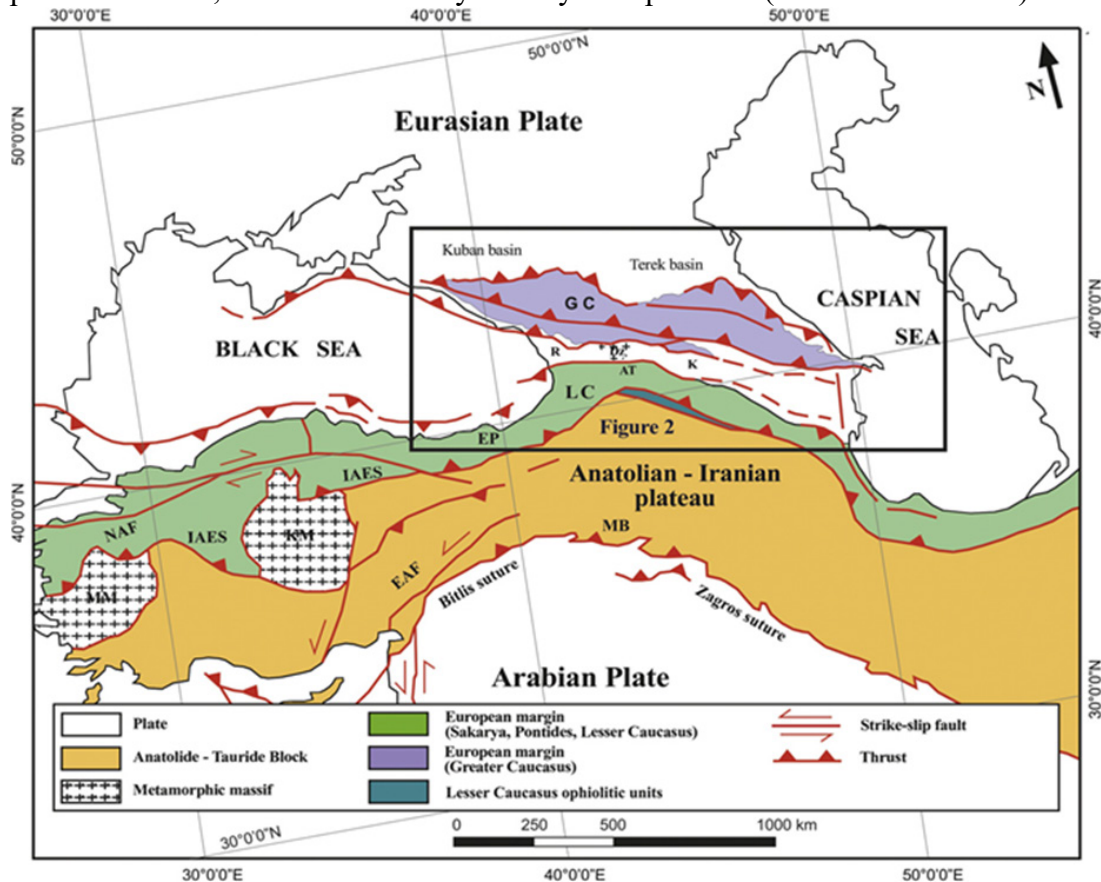


Figure 5: Tectonic map of the Arabia - Eurasia collision zone (modified from Sosson et al., 2010). Abbreviations: GC-Greater Caucasus; LC-Lesser Caucasus; AT-Achara-Trialeti; R- Rioni; Dz-Dzirula; K-Kura; MB-Mus Basin; EP-Eastern Pontides; KM-Kirsehir Massif; EAF- Eastern Anatolian Fault; NAF-North Anatolian Fault; IAES-Izmir-Ankara-Erzincan Suture; MM-Menderes Massif (N. Tsereteli, et al., 2016)

The Transcaucasian massif, previously part of the Thetys Ocean (Proterozoic - Early Cenozoic), formed an island-arc structure, confined during the Jurassic era between the Caucasian marginal sea towards north, and the Thetys basin toward south. The Thetys northward subduction developed an island arc. The structure, a classical arc-trench

system, worked as a west Pacific-type continental active margin. The area appeared as a low-level pelagic mountain range characterized by sedimentary, terrigenous and carbonatic, and volcanic deposition (Adamia et al., 1977). During the Lower Cretaceous, the movement reversed and the convergent phase began the Caucasus orogeny.

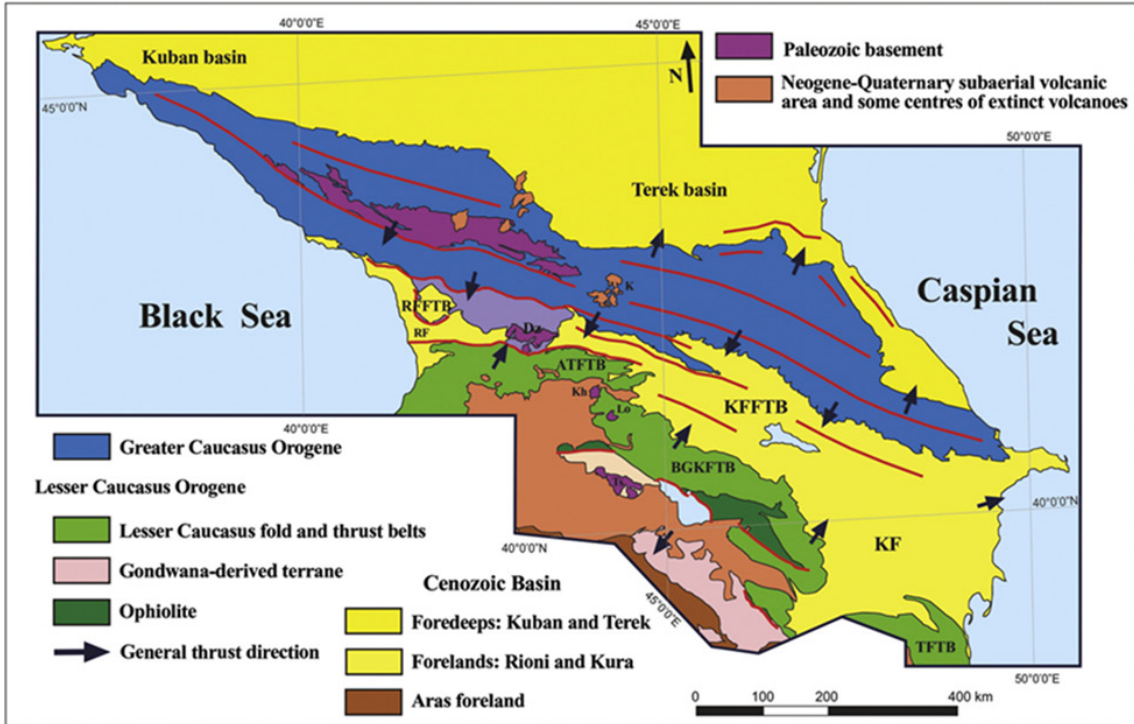


Figure 6: Simplified tectonic map of the Caucasus (Modified from Adamia et al., 2011a, 2011b; Mosar et al., 2010). Abbreviations: RFFTB-Rioni foreland fold and thrust belt; RF-Rioni foreland; KFFTB-Kura foreland fold and thrust belt; KF-Kura foreland; ATFTB-Achara-Trialeti fold and thrust belt; BGKFTB-Baiburt-Garabagh-Kaphan fold and thrust belt; TFTB-Talysh fold and thrust belt; DZ-Dzirula; Kh-Khrami; Lo-Loki; Ts-Tsakhkuniats; K-Kazbegi. (Tsereteli, et al., 2016)

The compression produced the collision between the Iranian-Turkish microcontinent and the volcanic arc forming the Lesser Caucasus. Moreover, at the beginning of the Tertiary period, the subduction of the Thetys crust under the new born Lesser Caucasus gave way to a new configuration to the area: creating a new big island-arc system, followed by an uplift and flysch deposition. The formation of the Lesser Caucasus island-arc is accompanied by volcanism in the central part, on the Iranian-Turkish microcontinent side, and the rift of the back-arc area corresponding to the Greater Caucasus oceanic basin with production of basalts. In the Oligocene all the Thetys crust was consumed and the ocean basin was enclosed. The Caucasus orogeny is considered to start at this point in geologic time. During the Miocene, the part between the Lesser and the Greater Caucasus was characterized from the formation of Rioni and Kura basins (Figure 6). Being a non-uniform continental collision, the central eastern part of the Great Caucasus is different from the western one that is, today, still part of an active margin characterized by

subduction. The actual morphology is the outcome of the uplift and erosion in the Late Pliocene.

The actual structure from south to north is exposed in Figure 7.

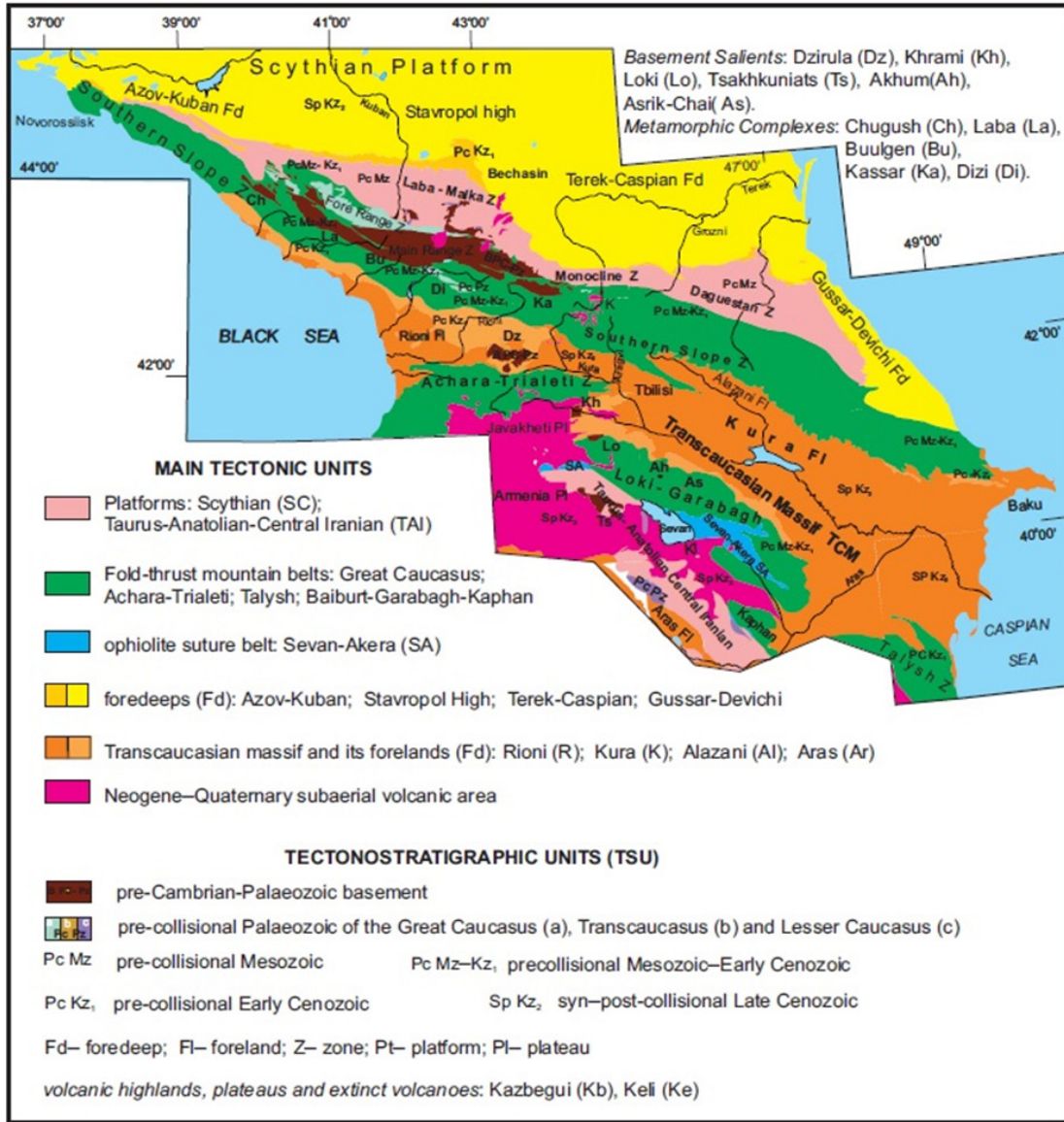


Figure 7: Geology of Caucasus, a review, Adamia et al.,2010

Along the western side of the Caucasus are signs that the subduction of the oceanic crust under Eurasia are still active, in fact there is even evidence of volcanism along the range (see Mt. Elbrus and Mt. Kazbegi). The eastern side of the Caucasus are signs of

continental collision. The middle portion is dissected by a transcurrent fault, oriented NNE.

#### **2.4.2 Geology of Enguri Dam Area**

The Enguri Dam is located among the foothills of the Caucasians (Georgian name for the Greater Caucasus). The area is deformed by weathering and tectonic folding and has a southern convergence. The lithologies around the dam are all part of the Rioni Basin series (Figure 8), more specifically of the Dizi series, composed by volcanic and sedimentary deposits from Jurassic to Quaternary. The area analyzed is almost 12 km N-S by 7 km E-W and includes all the slopes around the reservoir. The geological and geotechnical survey has been realized just on the Georgian side, along the east side of the reservoir; on the west side it was not possible to cross the border to reach the separatist region of Abkhazia due to safety concerns. All the Dam area appeared pervasively folded, characterized by very weak and fractured layers. A principal road for transportation, the Zugdidi-Jvari-Mestia-Lasdili road runs along the eastern side of the reservoir. Because of the orientation of geologic formations, this road and the reservoir effectively cuts across all the lithologies along the steep slopes. The layers appear weak and fractured with several springs appearing along the road cuts. The road conditions are hazardous since it is one of the busiest roads in Georgia and there are numerous, and sometimes massive, rock falls every day. As of now there are practically no mitigation measures to protect the reservoir, road, and travelers, except for some small concrete retaining walls and rock-filled cages to catch small amounts (few cubic meters) of mass movements. There are no retaining techniques to preserve the outcrops and keep the road safe. The lithologies observed during the geological survey are (Figure 8 and Figure 9):

- Jurassic (174-145 Ma): Middle and Upper Jurassic shallow marine terrigenous and carbonate rocks and Calc Alkaline basaltic and andesitic shallow marine volcanic rocks. Variegated, dark brown, red and green clays, white gypsum inclusions, weathered dark sandstones, micro conglomerates, debris of macadam of limestone with loam filler;
- Cretaceous (145-66 Ma): Lower and Upper Cretaceous shallow marine carbonate rocks, terrigenous clastics and turbidite;
- Tertiary- Quaternary: marine molasse, shallow marine, lagoon and continental rocks. Euxinic-basin rocks.

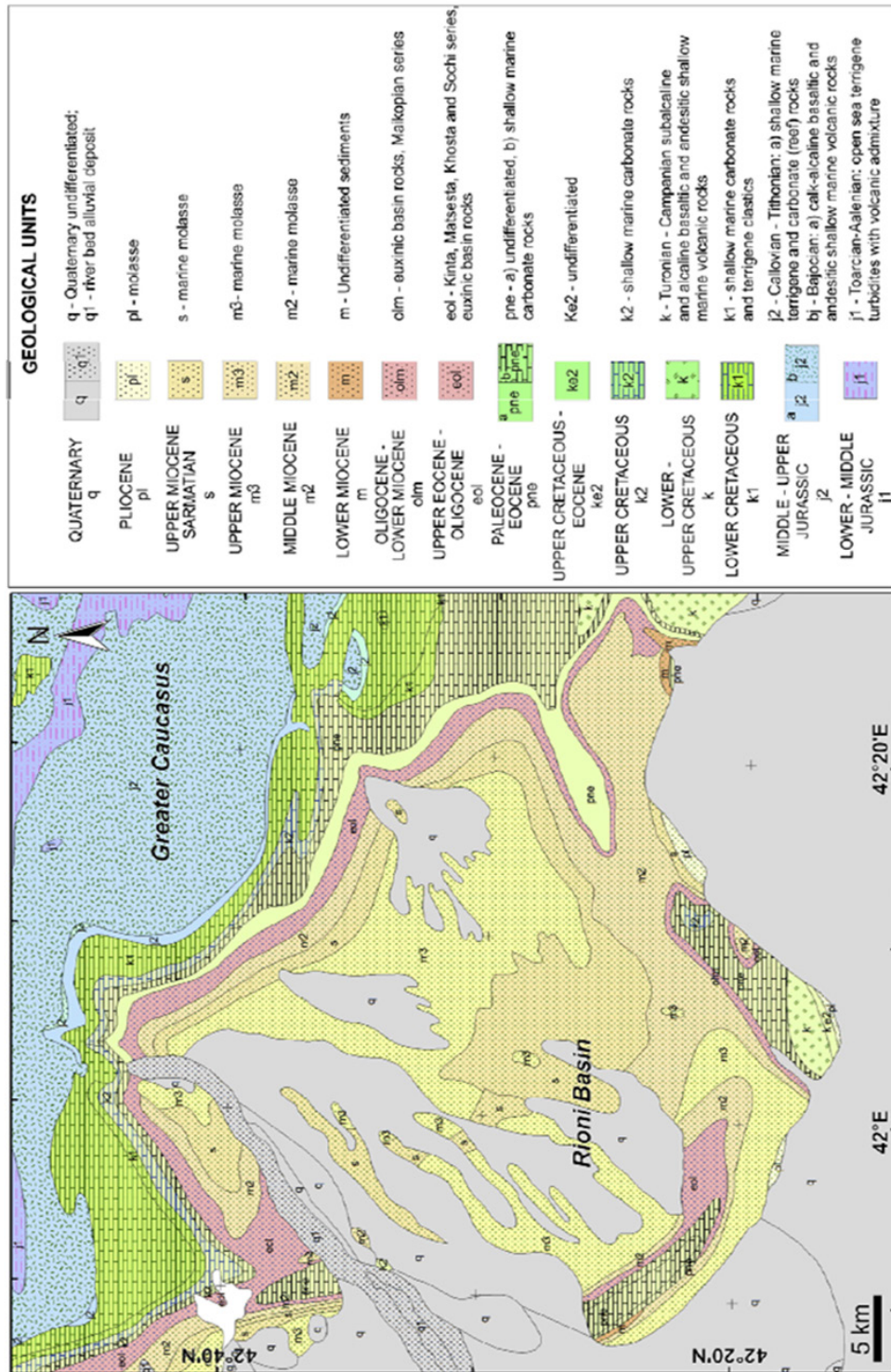


Figure 8: Geological map of the studied area (Adamia and Gujabidze, 2004)

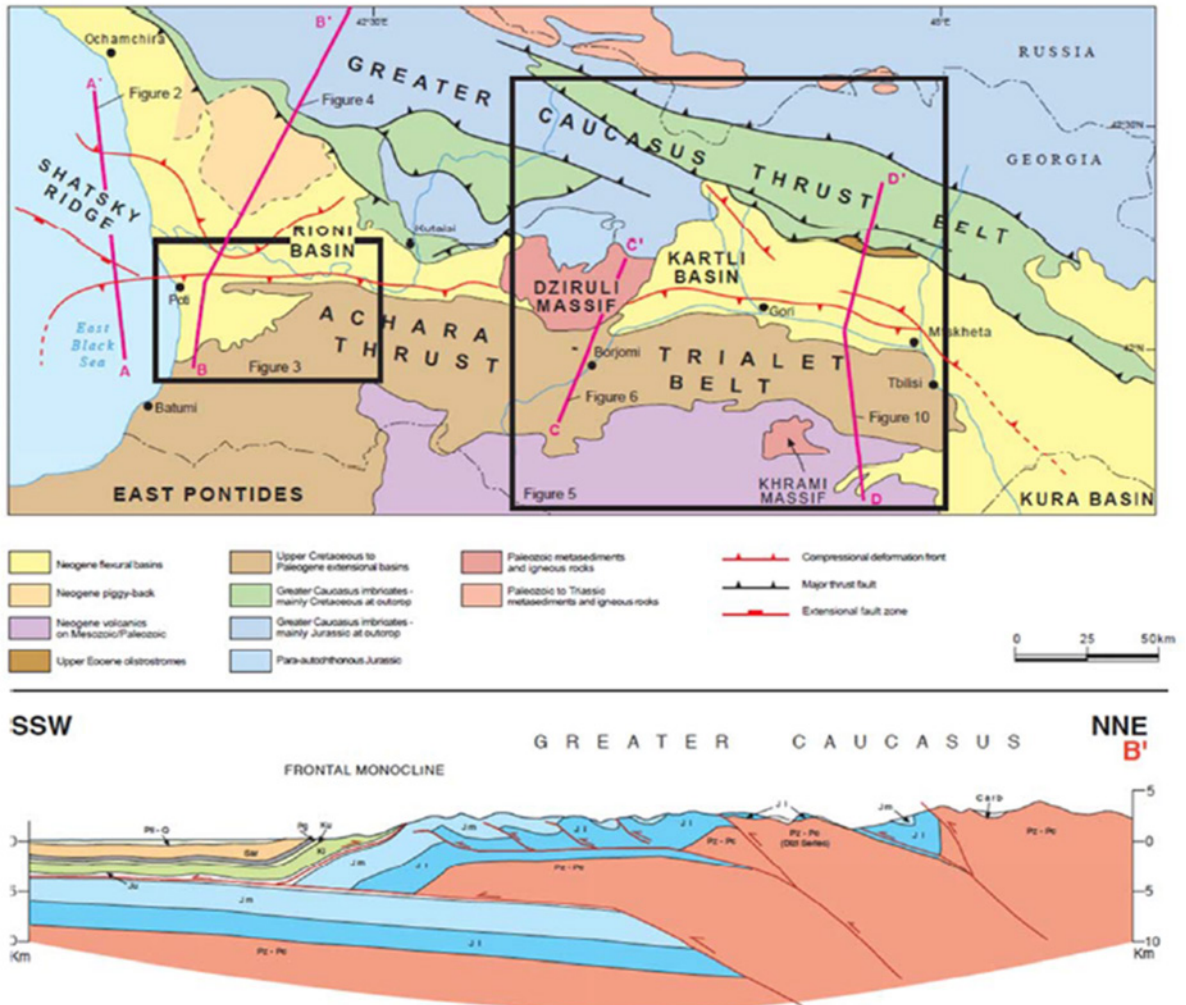


Figure 9: Main tectonic elements, locations map and geological section (C. J. Banks et al., chapter 17)



## **3 Methodologies**

### **3.1 Previous Data Collection and Processing**

Analysis of the area started with compiling and examining existing spatial data using Esri ArcGIS 10.3.1 software. The objective of the first phase of this work was to survey the slopes adjacent to the reservoir to better understand where large and potentially catastrophic landslides might occur and plan our fieldwork to measure geotechnical properties that would be use subsequently in the slope stability modeling.

#### **3.1.1 Structural Data from Tbilisi University**

The Georgian research group from the M. Nodia Institute of Geophysics (Tbilisi, Georgia) provided the structural and morphological data for all the Georgian territory. The data consists of shapefiles projected in Pulkovo\_42 coordinate system (Figure 10):

- Lithology;
- Morphology and field aspect;
- Tectonic Structures;
- Exogenous geological processes;
- Rivers;
- Glaciers.

Analyzing on ArcGIS 10.3.1, all the above shapefiles made the situation clearer through the study of the tectonic and water conditions as well as the morphology. It was decided to simplify the data layers to be more understandable by re-projecting and processing just the most useful and fundamental layer: the lithology shapefile (Figure 11). Projected in WGS\_1984\_UTM\_Zone\_38N Northern hemisphere, the shapefile was analyzed and modified, focusing just on the area needed. The layer shows six different lithologies, from Jurassic to Cretacic periods: Tuff, Tuffogenic Sandstones, Marls, Limestones, Conglomerates and Clays.

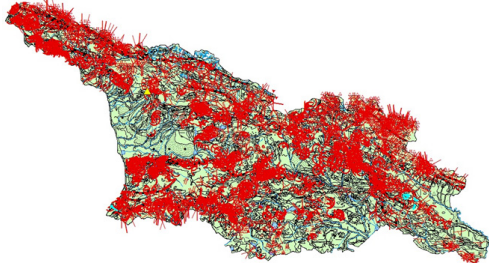


Figure 10: Complete view of the arcMap shapefiles from Tbilisi University

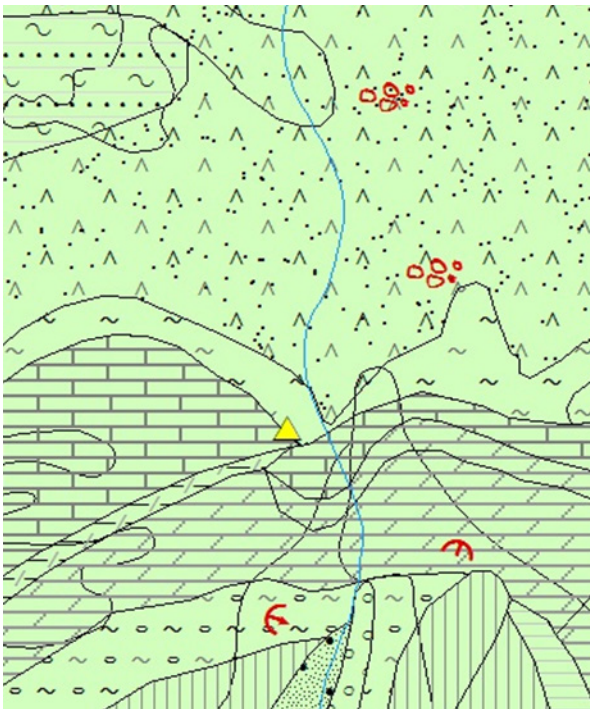


Figure 11: Zoom of the study area on arcMap showing the lithology layer and some geomorphological structures (data from M.Nodia Institute of Geophysics)

### 3.1.2 USGS ASTER Global DEM

The ASTER Digital Elevation Model (DEM) was downloaded from the Earth Explorer web page of the USGS website at 30-meter spatial resolution (GeoTiff, 1 arcsecond, projected in WGS\_1984\_UTM\_Zone\_38N Northern Hemisphere). The plan was to overlap the DEM with the lithology layer obtained from Tbilisi State University to compare the different lithologies with the different area of the dam reservoir, but there were problems about the overlapping due to the Z-factor value. When the Z-factor is set wrongly, the hillshade images appeared heavy or leaden. The Z-factor has been set based

on the latitude. Downloading the DEMs in raster format, the spatial reference is generally a geographic coordinate system instead of a projected coordinate system. Creating a hillshade from a DEM using default values for the data processing often produces a result that looks molten or over-processed because linear units cannot be defined for geographic coordinate systems. The fundamental problem occurs when the linear units for the geographic coordinate system are different from the Z units for the DEM. This problem can be avoided following two different strategies: project the DEM to define the linear unit or use the optional Z-Factor parameter in the hillshade tool. After processing the DEM, maps of the slope and aspect were generated to provide a better landscape-focused view of the area. Both were created using the Spatial Analyst Tools with ArcGIS. The aspect calculation gives information about the convergence of the slopes, about how they are directed on the lakeshores. The result shows how both the outcrops on the lakesides are convergent toward the reservoir. The slope (m) was reclassified in five classes, with a gradient that goes from  $10^{\circ} \leq m \leq 71^{\circ}$ , the aspect maintains the original classification. The slope map shows the relative steepness of the slopes. Along the reservoir shore the bedrock outcrops are especially steep, showing an inclination greater than 30 degrees almost everywhere. Comparing the slope and the aspect map with the Google Earth imagery makes it possible to visually identify the most vulnerable slopes (Figure 12).

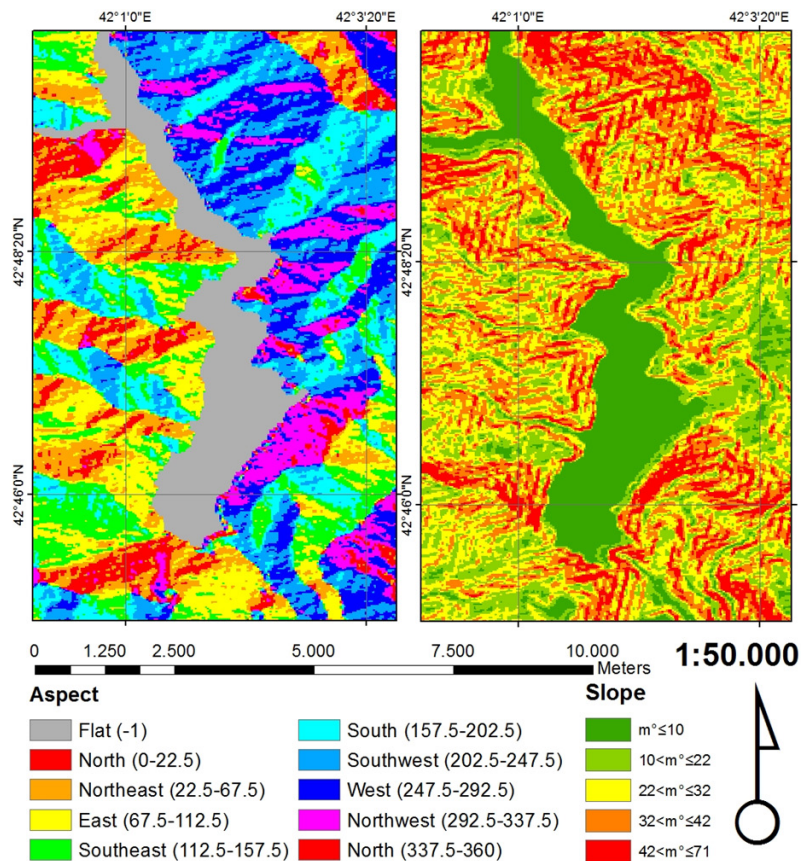


Figure 12: Aspect and Slope map of the area from arcMap 10.3.1. Realized from M.D. Acciaro, Scale 1:50.000

### 3.1.3 GPS Positions of the Sliding Zone

During the first “mission” to the Georgian dam in November 2015, the MTU team (represented at the meeting by John S. Gierke) was able to analyze the landslide-prone areas and register the main sliding positions with a handheld Global Positioning System device (Garmin GPS). All the waypoints and tracks registered were exported from GoogleEarth as .kml and taken on ArcGIS for being analyzed as shapefiles (Figure 13). Comparing the landslide points shapefiles to the slope and the aspect is confirmed that the slope-oriented West/Northwest and East/Northeast greater than 40° are the most likely to slide.

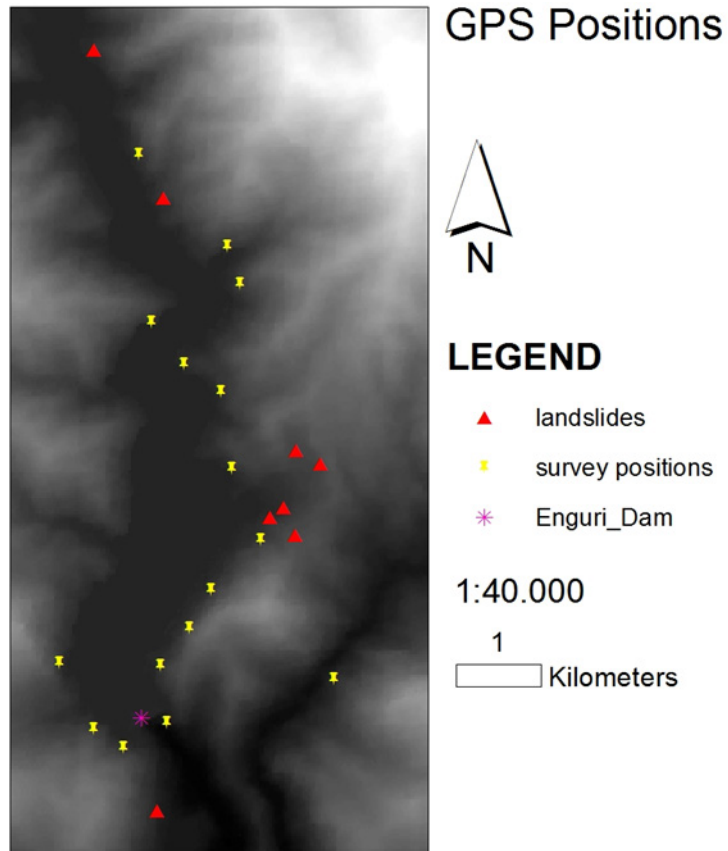


Figure 13: 1:40.000 scaled map of the GPS positions of the landslides area surveyed from J.S. Gierke on field

The result obtained is a shapefile layer, a distribution of points representing the georeferenced positions of all the evident sliding/falling areas around the reservoir on both sides. The ArcGIS file shows eight spots characterized by landslides on the outcrops around the reservoir. There are several typologies including: earth slides, rock falls, road slips, and relict landslides. The correlation among the slope map, the aspect map, and the sliding georeferenced spots helped us to better understand the surface condition of the area. Subsequently, adding the geological map information, the process helped us plan the field survey for the second mission to Enguri.

## 3.2 Field Investigation

The second mission to Georgia started on May 11 and ended on May 25, 2016. We planned the fieldwork by following the typical methodology:

- On-maps analysis of the area;
- Available data analysis on ArcGIS;
- Permits request to reach the sites;
- Lithological map analysis;
- Preparation of the equipment;
- GPS plan: choice of the locations to survey once on field using Google Earth and ArcMap

The fieldwork plan includes all the techniques used to survey the slopes, from the lithological analysis proceeding with the rock mechanics survey (table.4). The area interested is the oriental side of the reservoir, to reach the west side foreigners need a special permit from the Abkhazia government, unavailable option for our group with such small forewarning. The survey took place almost completely in the area between the principal road, the Zugdidi Jvari Mestia Lasdili, upslope, and the reservoir shore downhill. All the boreholes for the water level measurements, previously installed, were saturated once we reached the site (the survey overlapped with an intense rain period, so the springs and the waterfalls were forceful). The Slopes close to the reservoir and those that border the road (Figure 14) appear very weak: all the rock masses are highly fractured, and all the soils show signs of slip toward the reservoir. The clayey area of Khoko shows fresh swollen surfaces. Part of the road, the upslope with sliding clay mass, showed heavy signs of movement towards the downslope. Figures 16 and 17 show, the left lane (moving from south to north) has deeply sunk compared to the right one. Upslope of this area, a gypsum quarry was recently opened. The quarry is totally surmounted by deep fissures (1-2m deep) localized on the highest part of the Upper Jurassic slope. The principal concern for the local population is whether mining upslope of the Khoko landslide can be a problem for the security of the area. Other principal concern regards the all road portion set on the Cretacic limestones. The rocks are weak, highly fractured and unstable (Figure 15). All along the road, the outcrops run close to the lanes and, as Figure 14 shows, all rock falls continuously take place. The fallen rocks have diameters from a few centimeters to more than a meter, and the phenomenon is more frequent after rainy periods. Along the road, there is no evidence of structural/engineering intervention to reinforce the slopes or contain the rock falls. The fieldwork is just the first of many steps we went through to evaluate the vulnerability of the area. Investigating all the parameters we evaluate the possibility of potentially hazardous landslides that can endanger the Enguri power station and the watershed for the rivers Enguri and Magana.

The equipment used for the field survey is from the Michigan Technological University's Geological & Mining Engineering & Sciences department. For the different kinds of rocks, we used different kinds of instruments and methodologies. A geotechnical survey

is an analysis of soils and rocks throughout their aspect, their characteristics, and their physical parameters. The survey can furnish information about consistency, structure, groundwater and strength. It is possible draw out the various recommendations and instructions for the final technical project from the results. The work has been fairly standard for each lithology, but more concentrated and intense on the outcrops closer to the dam wall (Figure 18). Furthermore, along the road, precisely on three sites where the lithological limits run, the Georgian geophysicist David Odilavadze and his team conducted a Ground Penetrating Radar (GPR) analysis. The GPR is a geophysical method that uses radar pulses to image the subsurface; it works on three frequencies and has a receiver transmitter antenna type Zond-12e. The shielded antenna used had capacity of 100, 150, and 300 MHz. The scientists developed three profiles along and across the highway that shows the lithological change and the presence of water. During our field trip, we visited and analyzed 61 different locations: the quarry spot, the landslide locations, the borehole stations (BH), the sites analyzed with the ground penetration radar (GPR), and the outcrops of the geotechnical survey (letters A to T on Figure 18).



Figure 14: Fallen rocks at the border of the principal road



Figure 15: Example of a weak limestone outcrop



Figure 16: Road subsidence, evidence of Khoko landslide (1)



Figure 17: Road subsidence, evidence of Khoko landslide (2)

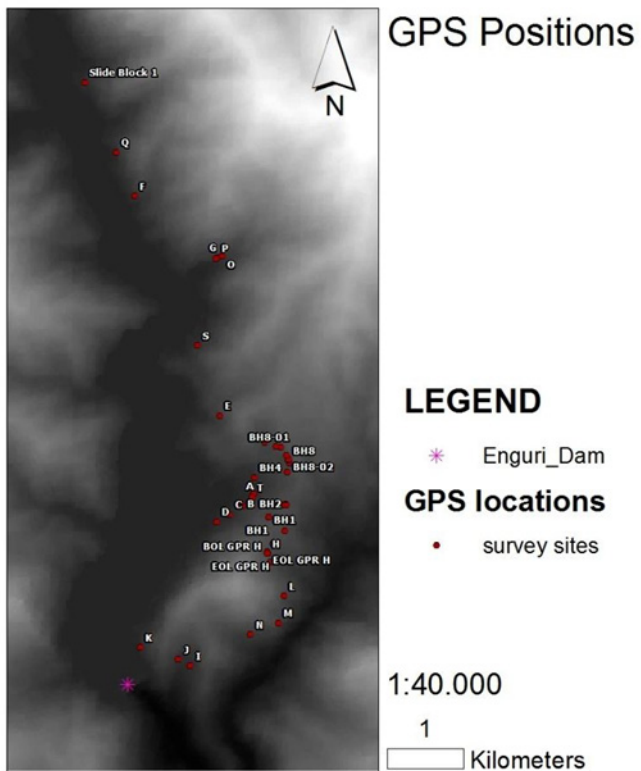


Figure 18: Map showing the GPS locations of the survey sites



### 3.2.1 Fieldwork on Rocks

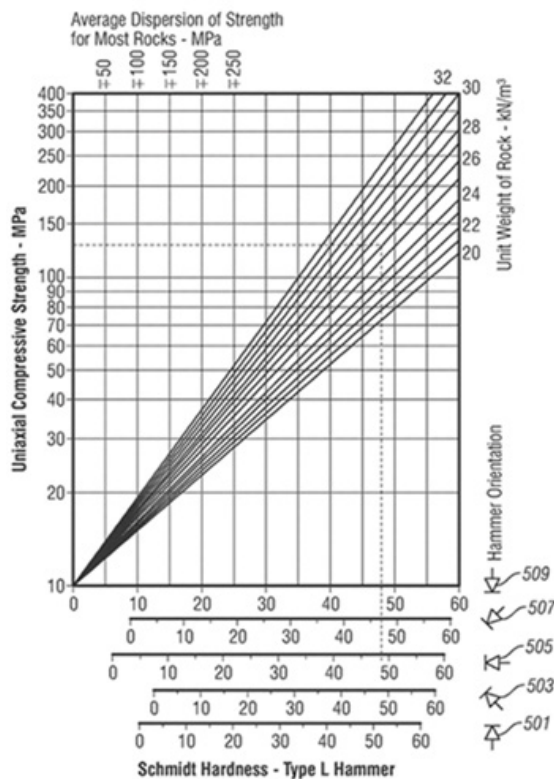
A rock mass is a volume that includes intact rock and discontinuities. In the area, there are different rock masses, disturbed by tectonic and weathering: Tertiary- Quaternary Marine Molasses and fluvial deposits, principally conglomerates, Cretaceous shallow marine rocks as limestones and Upper and Middle Jurassic Calc Alkaline volcanic rocks (see table.4). The area of interest is large and includes all of the lithologies cited above. We realized the survey gradually, schematically, to have a more precise and steady distribution of data.

The tools used for the geotechnical survey were various:

#### *Compass*

The compass measures strike and dip of geological features like layering and other discontinuities surfaces;

#### *Schmidt Hammer*



Originally made for concrete, the Schmidt Hammer (L type) is a device that evaluates the uniaxial compressive strength UCS of a rock through the measure of the rebound value, R. The device quantifies the rebound of a small spring-loaded mass against the material surface. The impact energy is constant, but the hammer evaluates the response of the material, determining its hardness and its resistance to penetration. We performed the test over each discontinuity surface. As mentioned before, the value obtained from a test with the Schmidt hammer is the rebound value R. R, corrected with the angle at which the measurement was carried out, can be correlated to the Unit Weight of Rock (kN/m<sup>3</sup>) using the standard chart (Figure 19). Once we had all the data, to make the job easier we carried out a formula useful to correlate immediately R to the UCS:

Figure 19: Schmidt hammer calibration chart

$$X = \frac{\text{LOG}(A) - \text{LOG}(B)}{60}$$

Through the formula above, we obtained different UCS values: for each rock, we calculate the UCS values following the Schmidt Hammer Orientation (Figure 20).

**A**= maximum UCS value obtainable for a given rock with a specific unit weight (250 in the example)

**B**= minimum UCS value for that kind of hammer orientation (18 in the example)

60= standard maximum value of R

$$UCS = 10^{X \cdot R + I}$$

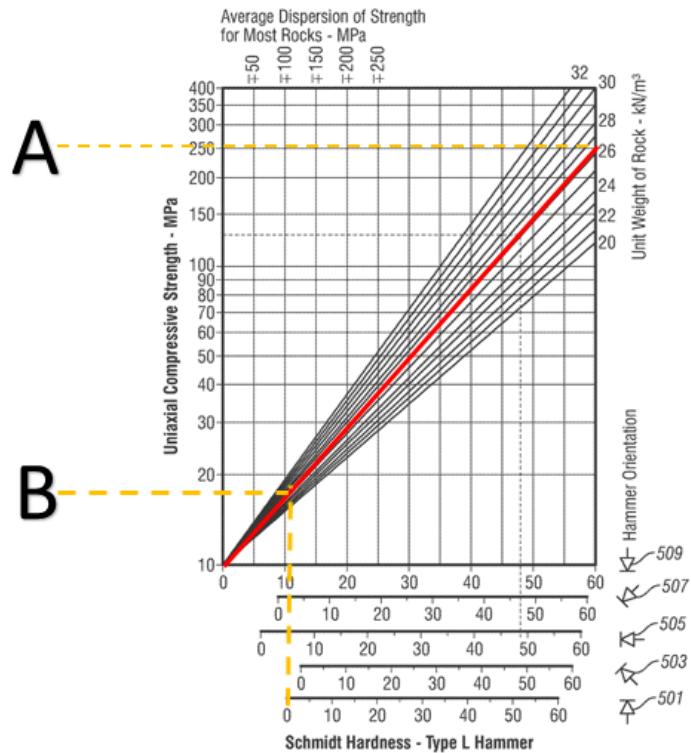


Figure 20: Schmidt hammer calibration chart instructions

For example, given 20 R-values surveyed with orientation 501 we obtained 20 UCS values. The average of all the UCS values for that 501-hammer orientation is then implemented in RocLab to evaluate cohesion and friction. There are UCS values from one to five for each rock, depending on which orientation is used (an average value for 501, 503, 505, 507 and 509 was used). The values obtained from the Schmidt Hammer test in the field are quoted in table.5.

### Point Load

The point load test (PLT) is used to determine the rock strength index on rock samples by compressing a sample between conical steel platens of a device until failure occurs



Figure 21: Point Load Test device from Michigan Technological University, department of Geological & Mining Engineering & Science

(Figure 21). The apparatus for this test consists of a rigid frame, two point load platens, a hydraulically activated ram with pressure gauge, and a device for measuring the distance between the loading points. The pressure gauge should be of the type in which the failure pressure can be recorded (J. Rusnak, C. Mark). Following the standard procedure from the International Society of Rock Mechanics (ISRM, 1985), starting from the  $I_s$  value, we evaluate the UCS and then friction ( $\Phi$ ) and cohesion ( $c$ ) using rocLab.  $I_s$  is the uncorrected point load strength index that must be corrected to the standard equivalent diameter ( $D_e$ ) of 50 mm, if the core's diameter is close to 50mm, like in our case, the correction is not necessary:

$$I_s = I_{s50} = \frac{P}{D_e^2}$$

Where  $P$  is the failure load (pressure\* $\pi$ \*piston area) and  $D_e$  is the equivalent core diameter. Before starting with the calculation of UCS, the  $I_s$  value must be converted from bar to MPa

$$UCS = K * I_{s50}$$

$K = 24$  is the constant conversion factor from Bieniawski, 1975 and Broch and Franklin, 1972.

Successively  $c$  and  $\Phi$  can be determined using Rocscience rocData, starting from the UCS value. The values obtained of field are shown in table 6.

### *Metric tape and rope*

The metric tape and rope was useful for measuring the water depth in the boreholes, the set spacing and the total spacing between discontinuities, and the dimension of the samples to use in the Point Load Test.

The geomechanical survey of the discontinuities follows the areal type. All over the reservoir, the outcrops were too steep, too covered with vegetation, or too dangerously subject to rock falls to be surveyed on foot, therefore we surveyed as much as we could in the most accessible areas. Almost all the windows we chose were from 5 to 10 meters long and about 5 meters tall. Once in the field we decided to survey the sites previously chosen on the maps continuing schematically, as mentioned above.

The first step was to give a general description of the lithology, giving information about general features like color, weathering, discontinuities, appearance, and principal structures; then we gave more information about the discontinuities and the physical parameters of the rock masse. Schematically:

#### General description:

- lithology and age;
- color;
- evidence of fossils, minerals or tectonic structures.
- conditions of the outcrop:
- appearance: massive R1, stratified R2, schistose R3, weak rock WR;
- rock mass alteration, W1 non-altered, W2, W3, W4, W5 totally altered (ISRM, 1981);
- weathering: unweathered, slightly, moderately, highly, completely, residual soil;
- water content: humid, traces of water, dry.

#### Discontinuities:

- number of families and orientation;
- termination;
- filling: empty, granular, cohesive, recrystallized;
- spacing: evaluation through measurement of a representative sample, average spacing, sortable in extremely close (<20mm), very close, close, moderate, wide, very wide and extremely wide spacing (>6000mm), ISRM, 1978.
- surface: rough or smooth the profilometer (Barton comb) was not available;
- blocks shape: polyhedral, equidimensional, prismatic, columnar, rhombohedral.

### 3.2.1.1 Quaternary-Tertiary

These lithologies characterize the area on the south side of the arch dam, so they are not part of the slopes around the reservoir. Anyway, the PISA-m model also includes part of that area, so we performed the survey on a conglomerate outcrop to find some basic parameters to implement in the model. The outcrop we surveyed is exactly composed by white colored, massive conglomerate sites on the area to the south of the dam wall. The sediment is part of the marine molasses and is located in a peculiar area. The zone is part of the Rioni Basin and is characterized by asymmetric river terraces (Figure 22) uplifted 150-200m compared to the valley floor. The Neogene and Quaternary terrigenous deposits rest on the substrate of carbonatic rocks of the Greater Caucasus (Tibaldi et al., 2016).

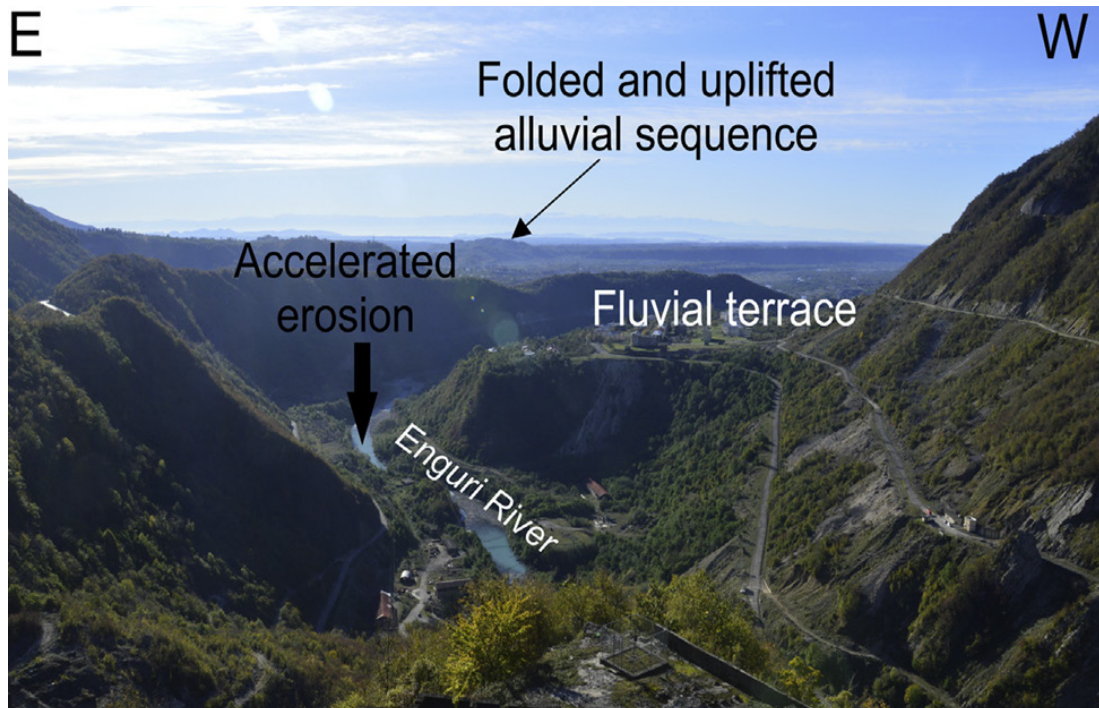


Figure 22: Geomorphological overview from Active inversion tectonics, simple shear folding and back-thrusting at Rioni Basin, Georgia. Tibaldi et al., 2016

The most recent deposits are loose fluvial materials (Figure 23). The conglomerates outcrop analyzed, instead, appear massive with some areas more altered and other less altered, dry, and characterized by high resistance to the Estwing hammer. In other places, further from our location, the outcrops look more loose, altered, and weak (chart1). Being a massive outcrop there is no evidence of discontinuities.



Figure 23: Neogene-Paleogene surveyed outcrop (picture from F.L. Bonali)

<b>Rock Mass (ISRM '78)</b>	Massive	Blocky	Tabular	Columnar	Irregular	Fractured	
<b>Structure</b>	R1 (Massive)	R2 (Stratified)	R3 (Schistose)	WR1 (Semi Coherent)	WR2 (Alternate)		
<b>Alteration (ISRM '78)</b>	W1 (no)	W2 (poor)	W3 (moderate <50%)	W4 (strong >50%)	W5 (complete)		
<b>Resistance (ISRM '78)</b>	R0 extremely weak 0.25-1 MPa	R1 very weak 1-5 MPa	R2 weak 5-25 MPa	R3 averagely resistant 25-50 Mpa	R4 resistant 50-100 MPa	R5 very resistant 100-250 MPa	R6 extremely resistant >250 MPa

### 3.2.1.2 Upper- Lower Cretaceous

The deposition of the shallow marine carbonates happened over all the Cretaceous period. The upper and lower cretaceous shallow marine carbonate rocks are pretty weak, white colored, fossiliferous, and highly disrupted by the tectonic events. From the Quaternary to the Cretaceous the stratigraphy is continuous almost everywhere around the dam, the area coincides with the north side of Rioni Basin. This lithology is part of a

big monocline at the roof of a south dipping thrust that grows from the main basal detachment, overlapping the Cretaceous sediments over the Jurassic once.

The tectonic activity of the area made all the outcrops highly fractured, stratified, folded and completely deformed (Figure 24), producing several discontinuity families and fractures.



Figure 24: Folded and fractured Cretaceous outcrop adjacent to the principal road

Evaluating the rock mass alteration, it was clear that the rocks were weak (chart2) due to the heavy alteration on the surface and inside of the discontinuities, however the rock was not well distributed such as a soil. Almost all the outcrops we surveyed were highly weathered (Figure 25), with traces of water in some spots. Many locations were almost impossible to survey because the rock was continuously crumbling and toppling down in variously sized pieces. The discontinuities on the carbonates are combined in five

different families. The terminations of the joints are of various type: ending in competent rock, connected to joints of other orientations, and protruding to the face outcrop. Almost all the discontinuities are empty with some silty or marly filling.



Figure 25: Detail of a Cretaceous outcrop

The average spacing between the discontinuities, following the ISRM'78 classification, ranged from extremely wide (>6000 mm) to fairly close (60-200 mm). Though we had no Burton Comb to evaluate the degree of roughness, the surfaces were determined to be slightly rough on average. In its totality, the outcrop presented polyhedral blocking with loose spacing between each surface (see GSI values in table 4).

<b>Rock Mass (ISRM '78)</b>	Massive	Blocky	Tabular	Columnar	Irregular	Fractured	
<b>Structure</b>	R1 (Massive)	R2 (Stratified)	R3 (Schistose)	WR1 (Semi Coherent)		WR2 (Alternate)	
<b>Alteration (ISRM '78)</b>	W1 (no)	W2 (poor)	W3 (moderate <50%)	W4 (strong >50%)		W5 (complete)	
<b>Resistance (ISRM '78)</b>	R0 extremely weak 0.25-1 MPa	R1 very weak 1-5 MPa	R2 weak 5-25 MPa	R3 averagely resistant 25-50 Mpa	R4 resistant 50-100 MPa	R5 very resistant 100-250 MPa	R6 extremely resistant >250 MPa

### 3.2.1.3 Upper- Middle Jurassic

The outcrops analyzed presented traces of Calc Alkaline basaltic and andesitic shallow marine volcanic rocks (Figure 26).





Figure 26: Upper Jurassic outcrop adjacent to the principal road

While the outcrops looked massive, un-weathered, and strong in some locations, they tended to be more loosely disrupted and weathered in others with increasing discontinuities throughout(chart3). The water amount varied as well. The sediments ranged from dry to having true water spillages.



Figure 27: Detail of an Upper Jurassic outcrop

The discontinuities had smooth surfaces and were unfilled. The spacing was narrow (Figure 27), goes from wide (600-2000mm) to extremely wide (>6000mm).

<b>Rock Mass (ISRM '78)</b>	Massive	<b>Blocky</b>	Tabular	Columnar	Irregular	Fractured	
<b>Structure</b>	<b>R1</b> (Massive)	<b>R2</b> (Stratified)	R3 (Schistose)	WR1 (Semi Coherent)	WR2 (Alternate)		
<b>Alteration (ISRM '78)</b>	W1 (no)	<b>W2</b> (poor)	W3 (moderate <50%)	W4 (strong >50%)	W5 (complete)		
<b>Resistance (ISRM '78)</b>	R0 extremely weak 0.25-1 MPa	R1 very weak 1-5 MPa	R2 weak 5-25 MPa	<b>R3</b> averagely resistant 25-50 Mpa	<b>R4</b> resistant 50-100 MPa	R5 very resistant 100-250 MPa	R6 extremely resistant >250 MPa



Figure 28: Middle Jurassic outcrop adjacent to the principal road



Figure 29: Detail of a Middle Jurassic outcrop

As Figures 28 and 29 demonstrate, the blocks of rock vary in shape but tend to be mostly prismatic and rhombohedral with exfoliation structures.

The Middle Jurassic deposits were older and harder to break with the hammer than other rocks in the area (chart4) resulting in high UCS values from the Schmidt Hammer. The PLT for core samples was not executed on the Middle Jurassic outcrops because the rock was too strong to be able to extract any cores. The rock was dark colored with no families of discontinuities determinable, but there was evidence of tectonic processes. The outcrop varied from primarily massive to blocky with a prismatic shape in some areas.

<b>Rock Mass (ISRM '78)</b>	Massive	Blocky	Tabular	Columnar	Irregular	Fractured	
<b>Structure</b>	R1 (Massive)	R2 (Stratified)	R3 (Schistose)	WR1 (Semi Coherent)	WR2 (Alternate)		
<b>Alteration (ISRM '78)</b>	W1 (no)	W2 (poor)	W3 (moderate <50%)	W4 (strong >50%)	W5 (complete)		
<b>Resistance (ISRM '78)</b>	R0 extremely weak 0.25-1 MPa	R1 very weak 1-5 MPa	R2 weak 5-25 MPa	R3 averagely resistant 25-50 Mpa	R4 resistant 50-100 MPa	R5 very resistant 100-250 MPa	R6 extremely resistant >250 MPa

### 3.2.1.4 Results

All the UCS values of the rocks are shown in the table below:

<b>STRENGTH OF ROCKS</b>	Neogene-Paleogene	Cretaceous	Upper Jurassic	Middle Jurassic
UCS from Schmidt Hammer on discontinuities surfaces	38740,97 KPa	38457,6 KPa	43814,75 KPa	92384,4 KPa
UCS from Point Load Test on samples	61080 KPa	95475 KPa	60960 KPa	-
GSI	60	34	56	70

The Point Load Test is conducted on small samples where discontinuities do not generally pervade any of the outcrop, consequently, the rocks appeared much stronger in the results. The GSI, Geological Strength Index, is instead a qualitative estimation of the rock mass strength, so the value refers to the average appearance of the outcrops.

### **3.2.2 Fieldwork on Soils**

A soil is an aggregate of loose or tied particles characterized by permanent or nonpermanent binding forces. A soil can be analyzed as a solid structure, even though it is a multiphase system composed of a solid, liquid, and a gaseous part, or as an aggregate. Characteristics such as dimension, size, or shape of single grains can be explored as well as the reaction to handling. Soils can have coarse or fine-grained material and are classified as organic when they are rich in organic components.

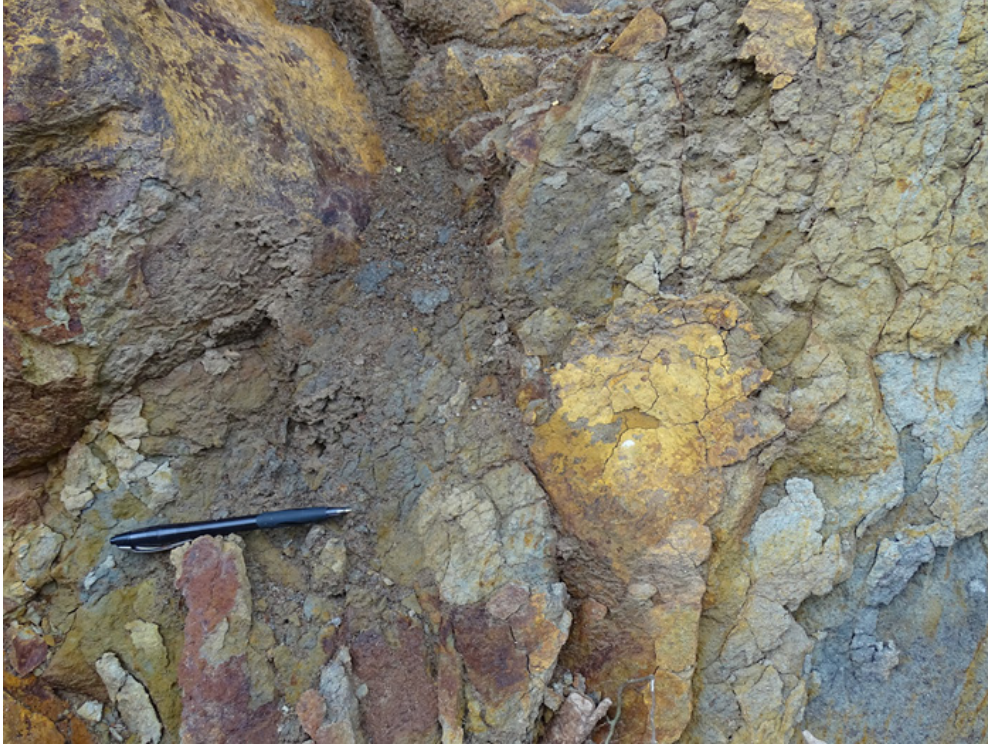


Figure 30: Clay mass over the sliding area characterized by gypsum inclusions

In the field, the geotechnical survey for a soil requires different determinations:

- Granulometry: visual examination of the percentage of different granulometries;
- Lithology: sand, marl, clay or intermediate typologies;
- Alteration: from really low, WC1, to really high, WC5;
- Color: hue, value and chroma;
- Structure: stratified, laminated, cracked, striated, blocky, lenticular, or homogeneous;
- Cementation and thickening: how simple it is to dig into the soil;
- Plasticity: handling, resistance at the repeated formation of a stick;
- Consistency: evaluation of the uniaxial compressive strength evaluated with the CPT, cone penetration test;
- Undrained cohesive strength:  $C_u$  evaluated with Torvane shear test,
- Organic component: woodiness, ordinary vegetation, smell;
- Humidity: evaluation of the water content, a soil can be dry, humid, wet, dripping or characterized by water discharge.

The Upper Jurassic soils in the Enguri area (Figure 31 and 32) includes variegated, dark brown and green clays with white gypsum inclusions (Figure 30) as well as weathered dark sandstones, micro-conglomerates, debris of macadam of limestone with loam filler.



Figure 31: Gypsum quarry in the Upper Jurassic unit, over the south Khoko niche

The lithology varies between each location: some spots are characterized by muddier deposits while other places have extremely weak, silty, planar layers with alternating sandy levels, in other locations, there are accumulations of shale chips that range from gray to green to red in color. The survey was conducted following the typical earth and soil geotechnical survey (survey data on tables 8 and 9). The tools used, furnished from the Michigan Technological University, are a Cone Penetrometer Test (CPT), and a Field Vane Shear Apparatus.



Figure 32: Detail of an Upper Jurassic loose outcrop

### *Cone Penetrometer Test*

The Cone Penetrometer Test (Figure 33) is one of the most effective in-situ test methods and can be applied for estimating soil parameters such as the undrained shear strength,  $S_u$  or  $C_u$ . The CPT in the story has mainly been used for three applications: estimating soil properties through appropriate correlations, directly performing geotechnical design, and determining subsurface stratigraphy.



Figure 33: Cone Penetration Test (CPT) device on the left and Shear Vane device on the right. Machines from the Geological & Mining Engineering & Science department of the Michigan Technological University



Figure 34: Press used for the calibration of the CPT device, laboratory of geotechnics of the Geological & Mining Engineering & Science department of the Michigan Technological University

lb (calibration)	inches		
0	0		
10	0,0071		
20	0,01415		
30	0,0201		
40	0,02645		
50	0,0325		
60	0,0382		
70	0,0452		
80	0,051		
90	0,05735		
100	0,06305		
	0,000626136 m		y=mx+b
	0,000975 b		

Figure 35: Excel file screenshot of the values used for the calibration of the CPT device

The CPT device shown in Figure 33 provided from the Michigan Technological University Department of Geological and Mining Engineering and Science had been calibrated in the laboratory before the fieldtrip using a press (Figure 34). The calibration gave a constant increment of weight (lbs) per increment of lowering (in); values are shown in Figure 35.



Given  $x$ =pounds (lb) and  $y$ =inches (in) we create a line linear equation (0, 0)

$$y=mx+b$$

(With  $m$ =slope and  $b$ = $y$ -intercept)

$$x=\frac{y-b}{m}$$

that we can define as  $Q_c$ , the corrected cone resistance:

$$Q_c=\frac{inches-b}{m}.$$

Given the total vertical stress in situ,  $\sigma_v = 0$ , the constant cone factor,  $N_k = 9.6$ , and the area

$A_c(\text{in}^2) = 1$  we can obtain the cone resistance  $q_c$ :

$$q_c=\frac{Q_c}{A_c}=Q_c$$

and the Undrained Shear Strength in pounds per square inch (psi)

$$S_u=\frac{Q_c-\sigma_v}{N_k}.$$

The friction is  $\Phi=0$  and the cohesion is equal to  $S_u$ , converted in MPa.

The results are shown in table 8.

### *Field Vane Shear Test*

The Field Shear Vane Test method (Figure 33) provides an in-situ undrained shear strength value for saturated fine-grained soils including clays and silts. The test is applicable to soils with undrained strengths of less than 200 kPa (ASTM D2573 / D2573M) and soils that are too sensitive can be rehashed with the vane insertion. This test method is used to evaluate the strength of undrained, fine-grained clays and silts. The vane shear strength values are, on average, higher when associated to other tests.

The device was calibrated using the calibration curve furnished by Michigan Technological University. The curve is used to calculate the line coefficient:

$$y=mx+q$$

$$m=\frac{y_2-y_1}{x_2-x_1}$$

having all the values of y (deflection), m and x (torque) is possible to evaluate q.

Being  $SV=y$  the Deflection in degrees:

$$SV=m*torque+q$$

and being  $T=x$  the Torque in ft-lbs:

$$T=\frac{SV-q}{m}$$

To calculate the cohesion, assuming the friction  $\Phi=0$ , first we need the standard value of the diameter:

$$D(\text{inch})=\frac{3}{4}=0.75 \rightarrow D(\text{ft})=0.0625$$

then is possible to evaluate undrained cohesive strength (cohesion):

$$Su \text{ (psf)}=\frac{6T}{7*3,14*D^3}$$

with  $Su \text{ (psf)} \rightarrow Su(\text{Mpa})= c(\text{MPa})$ .

Performing a subsequent back analysis, the friction value is assumed to be 30°.

The results are shown in table 9.

### 3.2.2.1 Results

The values surveyed in the field were homogeneous even if the survey was taken after a heavy period of rain. The value of friction was assumed to use the standard formula is 0

but, after a back analysis the friction is set to equal to 30°. The results are shown in the following table:

	Neogene		Cretaceous		Upper Jurassic soils		Upper Jurassic rocks		Middle Jurassic	
	c	$\Phi$	c	$\Phi$	c	$\Phi$	c	$\Phi$	c	$\Phi$
<b>avrg.</b>	0.29	42.28	0.22	35.01	0.01	30	0.46	50.21	0.65	55.18
<b>st.dev</b>	0.52	53.48	0.59	52.53	0.14	0	1.86	64.97	2.20	66.05
<b>max</b>	0.38	47.68	0.35	43.37	0.06	30	0.91	57.95	1.26	61.3
<b>min</b>	0.07	3.08	0.10	5.16	0.04	30	0.37	4.19	0.48	3.4

### 3.3 Landslides Analysis

As defined by Cruden in 1991, a landslide can be described as the movement of a rock mass, debris or earth down a slope. In 1978 Varnes gave another definition of the process, defining a landslide as “a downward and outward movement of slope forming materials under the influence of gravity”. The process is not as simple as it looks, a landslide can assume different shapes and involve deeper levels through complex processes. There are many triggering factors such as water, slope, roots, temperature, stress and strength of the material, anthropic intervention, etc... In recent decades, many efforts have been made to assess landslide susceptibility on a regional scale using different models and various methods for the different typologies. The first step should be the model evaluation: there are several kinds of landslides and different models to use for each of them. As reported by Frattini, Crosta and Carrara in 2009, the approval of a model needs to satisfy three criteria:

- conceptual and mathematical adequacy in describing the system behavior;
- data sensitivity;
- accuracy in predicting the observed data.

Considering a physically based model, we need to assess if the chosen model provides a physically acceptable explanation of the field observations. The first evaluation of the model must be based on how well the variables describe the process no matter which model, statistical or an empirical, is used. The accuracy is represented by the ratio between the results obtained and the observed data and is fundamental to the model. There is a simple method to assess the accuracy that uses a binary classification of

susceptibility in stable and unstable units. This classification requires a cutoff value of susceptibility that divides stable terrains (susceptibility less than the cutoff) and unstable terrain (susceptibility greater than the cutoff) (Frattini et al. 2009). Comparing the forecasting with the effective observations is a way to implement the statistics and evaluate the accuracy of the susceptibility model. There are many other methodologies to implement the statistics, for example ROC and Cost Curves.

	<b>PREDICTED stable -</b>	<b>PREDICTED unstable +</b>
<b>OBSERVED stable -</b>	<b>true negative -\-</b>	<b>false positive +\-</b>
<b>OBSERVED unstable +</b>	<b>false negative -\+</b>	<b>true positive ++</b>

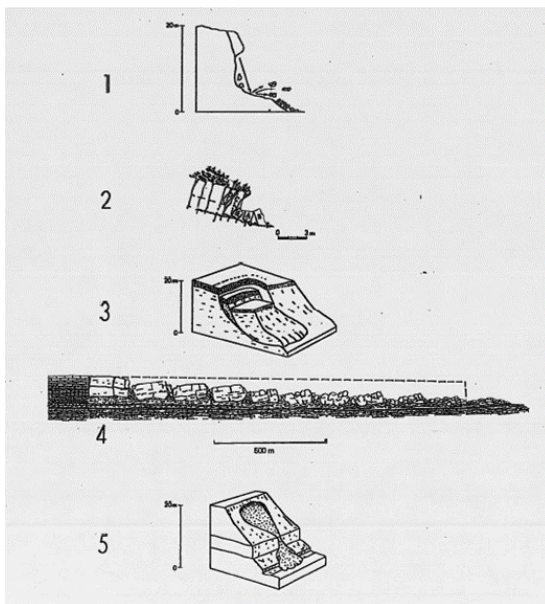


Figure 36: Basic classification of landslides: 1. Fall, 2. Topple, 3. Slide, 4. Spread, 5. Flow (Cruden and Varnes, 1996)

The landslides of the Enguri area are developed in rocks and in soils. In the Cretaceous limestones there are five different families of discontinuities that generate a weak structure characterized by topples and falls. In the Jurassic soils, there was evidence of deep-seated landslides, amenable to a nested rotational- earth flow with a curve deep detachment surface.

Firstly, we implemented the geomorphological analysis of the Khoko sliding area using Google Earth to trace the fractures, swelling, faults, hypothetical niches of detachment, and the drainage basin. The morphology of the area, in particular the shape of the central drainage watershed, showed that besides Khoko there was a bigger landslide that started from the northern-east mountain range. Tracing the contours Khoko seems to be just the final part, practically the foot of a bigger structure.

Using Google Earth, a tiff stereonet, and the grid Slope layer, we traced different niches of detachment: five over Khoko and four over the structure to the north.



Figure 37: Detachment niches of Khoko landslide (south) and of a hypothetical bigger structure (north)

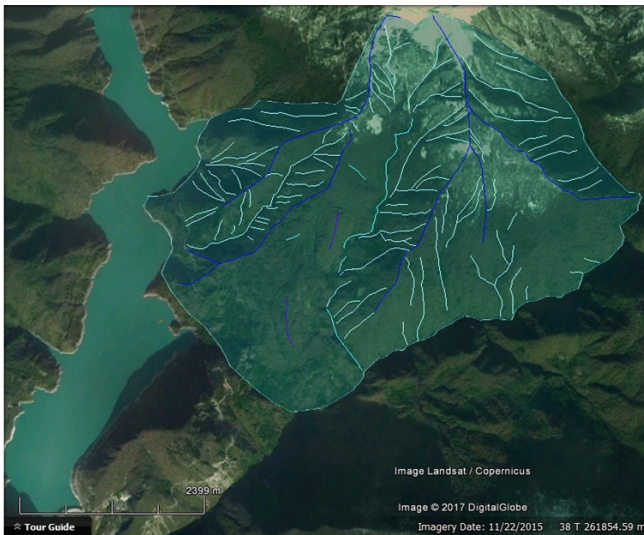


Figure 38: Drainage basin of the area. Light blue: flow pattern; dark blue: watershed

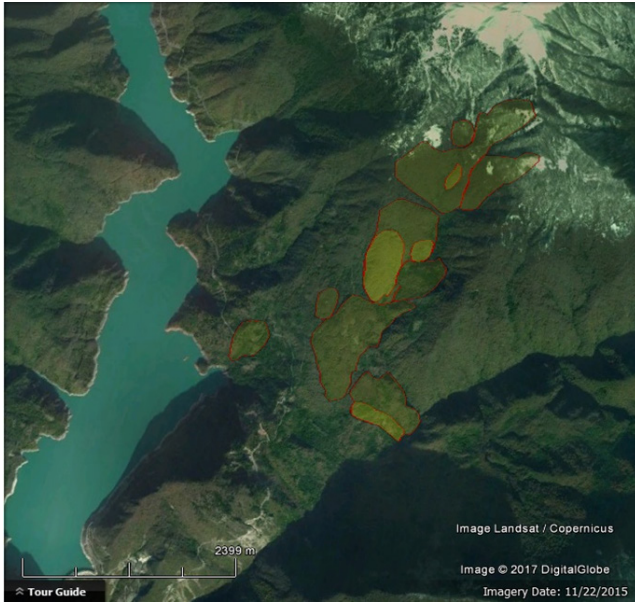


Figure 39: Smaller bodies and swollen areas identified over the hypothetical landslide



Figure 40: Fractures and general morphological discontinuities



Figure 41: Faults

The most obvious sign of a bigger primary slide (apart from the obvious signs such as fractures) was the drainage morphology. The south-west movement obliterated the central watershed that now is recognizable by analyzing the adjacent structures. The area showed interruptions in the drainage network and several bulges, however, we choose to concentrate the models on Khoko. First, we analyzed the Enguri reservoir area using the PISA-m software to evaluate the landslide susceptibility of the area and the surface movements in undrained conditions. Successively, we focused on the east side of the reservoir, Jurassic soils sliding area, where we studied a 2D section of the slope obtaining the finite elements analysis using Rocscience Phase2.

### 3.4 PISA-m

The plan was to build a susceptibility map of the area using the software PISA-m. The software calculates the average Factor of Safety for a forested infinite slope and perform a probabilistic static and seismic slope stability calculations starting from a digital elevation model. It is based on a first-order second-moment formulation of the infinite slope equation used by the U.S. Forest Service slope stability software LISA and DLISA which measures how trees roots affect the strength of a slope.

PISA-m requires four different input files: the DEM map (Figure 42), the lithological units map (Figure 43), the vegetation coverage map (Figure 44), and a results sheet. No matter which is used, the Arc format or the Surfer format, all three of the input maps must be ASCII files (.asc) and must have the same format and size. Maps of different sizes or geographic extent cannot be combined in a PISA-m run.

The landslide susceptibility analysis covered an area 11.7 km long and 6.7 km wide, which was determined in the field. The landslide prone area was catalogued according to lithologies, morphology, and the anthropic settlements around the Enguri reservoir. The DEM map used to create the dem.asc was derived from a 30m resolution Aster file from the USGS catalogue. The lithology map needed to create the soils.asc was hand drawn following the geological map of the area. The lithologies were also analyzed through a geotechnical survey in the field during the 2nd mission to Enguri Dam, in May 2016. The final layer, trees.asc, was obtained by processing a LANDSAT8. The vegetation coverage was created playing with the bands on ArcMap, and obtaining the NDVI, a layer that indicates the density of vegetation in an area. The obtained raster was then converted to ASCII similar to the other layers. The geological and geotechnical analysis showed all the ways a hypothetical landslide could affect the environment: the anthropic settlements safety, the water push toward the dam wall, the road stability, and the gypsum mine realization over the clays. In the next three paragraphs, there is an explanation of how the input maps for PISA-m have been determined; successively there is an explanation for the software operation and the landslide susceptibility modeling.

### **3.4.1 Digital Elevation Model**

The digital elevation model layer, shown in Figure 42, was derived from the 30m resolution aster file, processed and cropped to fit the software properties. The area covered ranges from 251m to 2135m above sea level. The DEM layer, as the lithology and forest coverage together, had to run in PISA-m as ASCII file (.asc). As previously mentioned, the software calculated the average Factor of Safety for a forested, infinite slope and performed a probabilistic static and seismic slope stability calculation for topography starting from a digital elevation model. The DEM was implemented as a map to provide the slope morphology and the altitude of the different zones. Similar to previous files worked on during this research, the DEM converted to ASCII was a 30 meter resolution raster with WGS1984 as the coordinate system. The scale was 1:50:000 and its dimensions needed to be the same as the other layers.



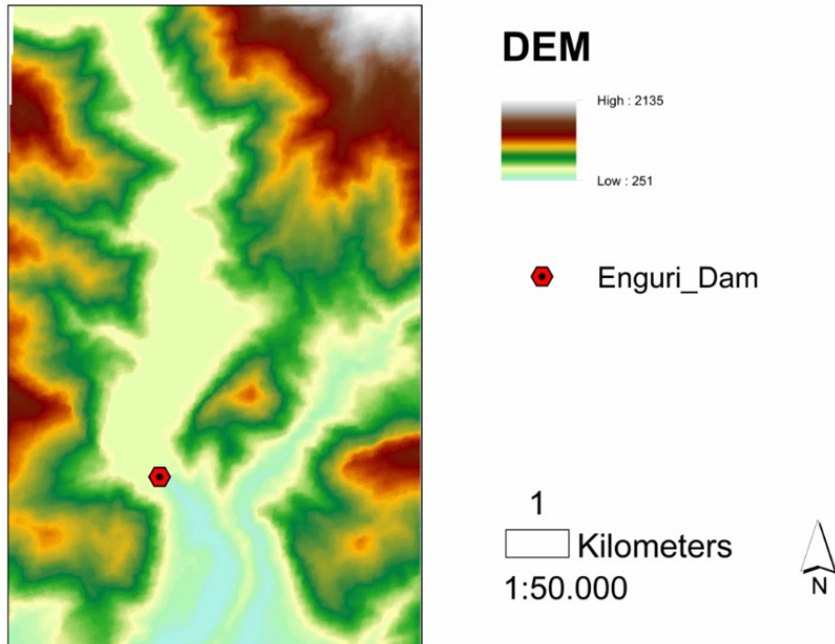


Figure 42: DEM arcMap map

### 3.4.2 Lithologies

The lithology layer in Figure 43 was created as a shapefile layer. The first step was to scan the original lithological map of the area as a raster layer and convert it to an ArcGIS file. After creating a new polygon feature class, drawing all the lithological layers and giving the exact projections, the product obtained was a shapefile containing all the attributes for each lithologic unit. To process the file, the software PISA-m required an ASCII grid format file, named soils.asc, The shapefile then had to be converted to a raster file (ArcToolbox> Conversion Tools> To Raster> Polygon to Raster) and then converted to ASCII (ArcToolbox> Conversion Tools> From Raster> Raster to ASCII). The resulting soil classes inserted in the parameters file, example.par, were:

- Quaternary- Neogene
- Cretaceous
- Upper Jurassic soils
- Upper Jurassic rocks
- Middle Jurassic rocks

The software ran an implementing average, standard deviation, and range of physical parameters for each lithologic unit.

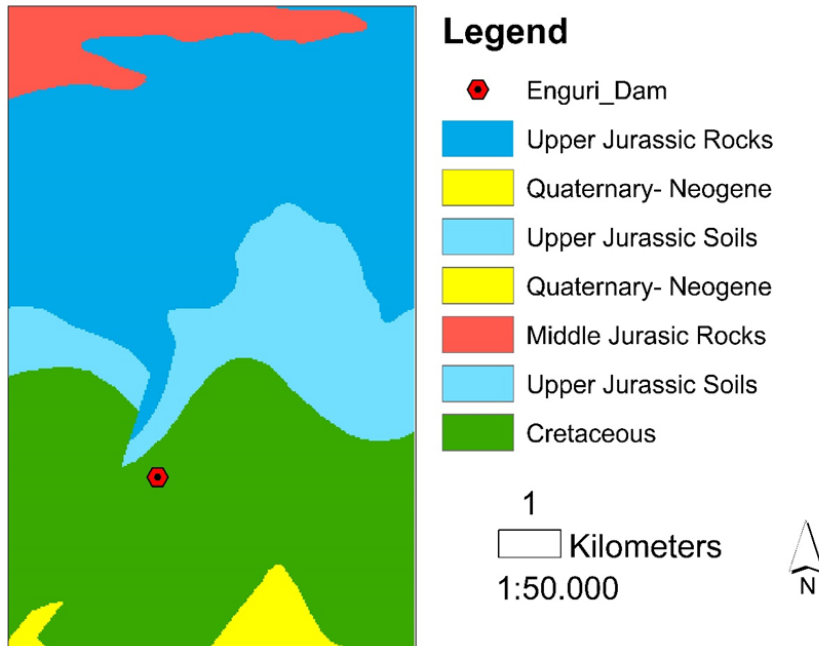


Figure 43: Lithologies arcMap map

### 3.4.3 Normalized Difference Vegetation Index

When light hits an object, some wavelengths of the spectrum are absorbed while others are reflected. To analyze the vegetation of an area we analyzed the wavelengths of visible and near-infrared sunlight that was reflected or absorbed by the plants. A leaf's structure reflects and absorbs sunlight through its pigment, chlorophyll, to conduct photosynthesis. The most common measurement of vegetation on digital maps is called Normalized Difference Vegetation Index (NDVI) shown in Figure 44. Values of NDVI that are lower than 0.1 correspond to absent vegetation, meaning sediments or snow. Intermediate values as 0.2 and 0.3 represent grass or sparse vegetation. High NDVI values like 0.6 and 0.8 indicate temperate and tropical rainforests (from Earth observatory page of NASA website [earthobservatory.nasa.gov](http://earthobservatory.nasa.gov)). To create an NDVI we processed the USGS Landsat data:

L8 OLI\TIRS (Operational Land Imager\ Thermal Infrared Sensor) ID:  
 Multispectral\_LC81720302015353LGN00\_MTL.

Landsat measures different ranges of frequencies, also known as bands, along the electromagnetic spectrum. The L8 datum consists of 11 bands: nine spectral bands with a spatial resolution of 30 meters (bands 1 to 7 and 9), one spectral band with resolution of 15m (band 8), and two Thermal IR bands with a spatial resolution of 100m:

- 1\_ Coastal Aerosol
- 2\_ Blue band

- 3\_Green band
- 4\_Red band
- 5\_NIR (Near Infrared)
- 6\_SWIR1
- 7\_SWIR2
- 8\_Panchromatic
- 9\_Cirrus
- 10\_TIRS1 (Thermal Infrared 1)
- 11\_TIRS2 (Thermal Infrared 2)

In summary, the NDVI described the vegetation cover by showing the difference between the red light (RED) absorbed by vegetation, and the near infrared (NIR) reflected by vegetation:

$$NDVI = \frac{NIR - RED}{NIR + RED}$$

By processing the bands, it was possible to create an NDVI layer displaying NIR:

- Band7 (NIR1), selected as the red channel
- Band5 (red band), selected as the green channel
- Band3 (green band), selected as the blue channel

The NDVI raster file was converted into an ASCII grid format file, similar to previous files, to run in PISA-m. The software considered Cohesive Strength and Tree Surcharge of the green covering shown in the NDVI layer.

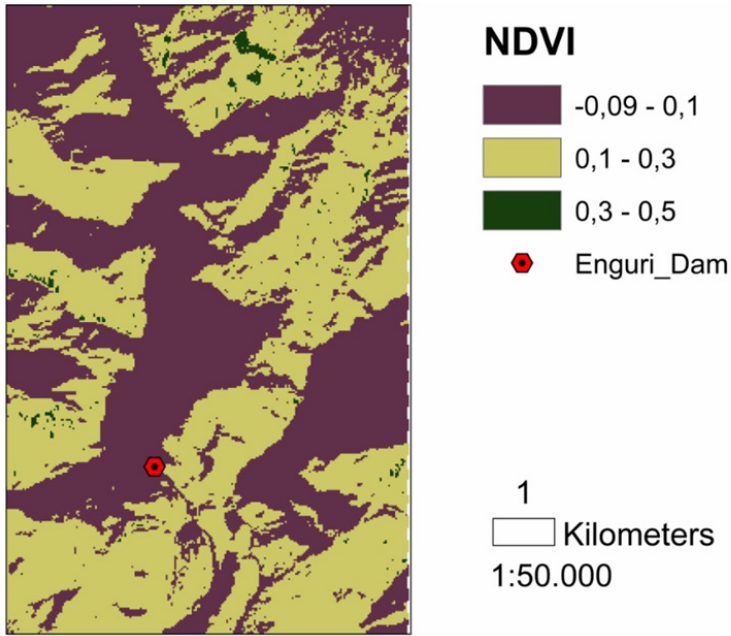


Figure 44: NDVI arcMap map

### 3.4.4 PISA-m: Map Based Probabilistic Slope Analysis

Generally, slope stability models are based on infinite slope idealization, however, there are no real slopes that can perfectly fit the model. For the most part, natural landslides are difficult to study meaning the approximation to a certain model is not always the correct method. Idealized structure is a fair preliminary analysis to understanding which area is in need of a more detailed study (Frattini et al., 2009). For our case of study, we used PISA-m to analyze the whole area. As explained in “PISA-m Map-Based Probabilistic Infinite Slope Analysis” Version 1.0.1, User Manual Updated March 2007, PISA-m is a map based probabilistic static and seismic slope stability analysis for a forested infinite slope. The formula that PISA-m implemented is shown in Figure 45:

$$FS = \frac{c_r + c_s + [q_t + \gamma_m D + (\gamma_{sat} - \gamma_w - \gamma_m) H_w D] \cos^2 \beta \tan \phi}{[q_t + \gamma_m D + (\gamma_{sat} - \gamma_m) H_w D] \sin \beta \cos \beta} \quad (1)$$

in which

- $c_r$  = cohesive strength contributed by tree roots (force/area)
- $c_s$  = cohesive strength of soil (force/area)
- $q_t$  = uniform surcharge due to weight of vegetation (force/area)
- $\gamma_m$  = unit weight of moist soil above phreatic surface (weight/volume)
- $\gamma_{sat}$  = unit weight of saturated soil below phreatic surface (weight/volume)
- $\gamma_w$  = unit weight of water (9810 N/m<sup>3</sup> or 62.4 lb/ft<sup>3</sup>)
- $D$  = thickness of soil above slip surface (length)
- $H_w$  = height of phreatic surface above slip surface, normalized relative to soil thickness (dimensionless)
- $\beta$  = slope angle (degrees)
- $\phi$  = angle of internal friction (degrees)

Figure 45: Factor of safety FS formula for a forested infinite slope (source: PISA-m manual, William C. Haneberg)

The software uses the first-order second-moment (FOSM) method to calculate the infinite slope equation. This is a probabilistic method used to determine the stochastic moments of a function with random input variables.

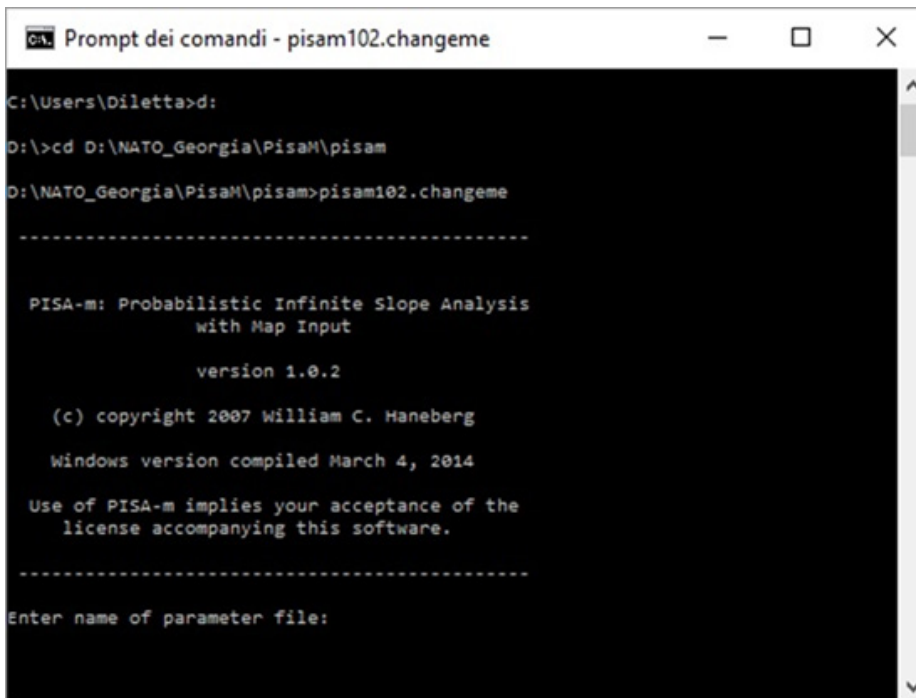
PISA-m ran under MS-DOS (Figure 46) and needed four input files to model the analysis:

- a DEM in map form (dem.asc, Figure 42);
- a lithological units map (soils.asc, Figure 43);
- a vegetation cover map (trees.asc, Figure 44);
- a parameter file containing all the physical parameters (FileName.par, Figure 47).

The final output was a file (results.asc, Figure 49) containing the resultant Factor of Safety (FS) value spatially distributed, where each pixel on the final map corresponded to a unique value of the FS. The result was in the form of an ASCII file, to be readable in GIS system and convertible to raster using arcMap.

The first map input, the DEM, contained information about the elevation, that is, a distribution of elevation values that goes from 251 m to 2135m in this case. The lithological units and the vegetation cover maps were composed by grids of integer values that correspond to items in the parameter file. Each value in the lithologic units map and vegetation cover map files correspond to an elevation value in the DEM input file. The three maps used to implement the software consist of a header followed by a grid of values that can be two different ASCII grid formats: either Arc ASCII grid format

or Surfer ASCII grid format. The Arc ASCII grid format was chosen for this project. Before the model was run, the format to be read to was specified avoid errors. Initially, the files were not ASCII files but raster and shapefiles, so they were converted using ArcMap. After the conversion, the layers were modified to make them equal: we revised the layer dimension, the number of rows (nrows) and columns (ncolumns), the coordinate system, the pixel number, and the cell size (DEM grid spacing). The information in the header lines had to be identical among the three input maps. If the maps had different sizes or different geographic extent, they could not be combined to run the model. The parameter file, as shown in Figure 47, has a “.par” extension and is compiled using the statistical distribution of the physical parameters of the area studied. All the physical values regarding the surface, the lithologies, vegetation, water, and the boundary conditions are implemented in the parameter file as numbers. Analyzing the parameter file input sheet (Figure 48) we can see that each line contains an information. The first line includes two different entries: “static” and “mean”.



```
Prompt dei comandi - pisam102.changeme
C:\Users\Diletta>d:
D:\>cd D:\NATO_Georgia\PisaM\pisam
D:\NATO_Georgia\PisaM\pisam>pisam102.changeme
-----

PISA-m: Probabilistic Infinite Slope Analysis
with Map Input

version 1.0.2

(c) copyright 2007 William C. Haneberg

Windows version compiled March 4, 2014

Use of PISA-m implies your acceptance of the
license accompanying this software.

-----

Enter name of parameter file:
```

Figure 46: Command prompt example to run PISA-m

```
static mean
in_format arc
out_format arc

dem.asc
soils.asc
trees.asc
results.asc

gw 9.810
an 0
dn 0
IA 0
minslope 10
z_err 10

soils

phi normal 0 0 0
cs normal 0 0 0
d uniform 0 0 0
h uniform 0 0 0
gs normal 0 0 0
gm normal 0 0 0

trees

cr normal 0 0 0
q normal 0 0 0
```

Figure 47: Parameter file (.par) example (source: PISA-m manual, William C. Haneberg)

The first entry, “static”, dictates whether PISA-m should implement a static or a seismic slope stability calculation. The second entry, “mean”, dictates which kind of results will be produced by the software, for example if the resulting Factor of Safety value is the mean, the standard deviation or the probability will be lower than one (<1).

Value 1	Value 2	Result Calculated
static	mean	Static factor of safety mean, $\overline{FS}$
	sd	Static factor of safety standard deviation, $s_{FS}$
	probability	Static probability of sliding (lognormal), Prob [FS < 1]
	reliability	Non-parametric slope reliability, $(\overline{FS} - 1)/s_{FS}$
seismic_a	mean	Newmark acceleration mean, $\overline{a}_N$
	sd	Newmark acceleration standard deviation, $s_{a_N}$
	probability	Probability that Newmark acceleration exceeds a user-specified threshold Prob[ $a_N < a_{crit}$ ]
	reliability	Non-parametric Newmark acceleration reliability, $(\overline{a}_N - a_{crit})/s_{a_N}$
seismic_d	mean	Mean Newmark displacement, $\overline{D}_N$ , in cm calculated using Jibson's simplified method
	sd	Option not available ( $s_{D_N} = \pm 0.375 \log \text{cm}$ )
	probability	Probability that the Newmark displacement exceeds a user-specified threshold Prob[ $D_N > D_{crit}$ ]
	reliability	Non-parametric Newmark displacement reliability $(D_N - D_{crit})/s_{D_N}$

Figure 48: Entries to implement the different calculations on PISA-m (source: PISA-m manual, William C. Haneberg)

The second and third lines are “in\_format arc” and “out\_format arc” and respectively tell which map format (arc or surfer) to read and write. The arc format was used in this case. The lines from 4 to 7 contain the four input file names and the output map name; they must have the name that we use to save the files and must be listed in this order to perform the analysis correctly.

The lines 8 through 13 contain the geotechnical parameters referred to as the general conditions of the area analyzed:



a) Physical Parameters legend	
gw	Unit weight of water (KN\m3)
an	User-specified Newmark acceleration threshold (g)
dn	User-specified Newmark displacement (cm)
IA	Arias intensity of the earthquake for Newmark displacement calculations (m\s)
minslope	Minimum slope angle (degrees)
z_err	DEM elevation error standard deviation (units consistent with the DEM)

b) Physical parameters legend	
phi	Angle of internal friction (degrees)
cs	Soil cohesive strength (pressure)
d	Soil thickness (length)
h	Pore pressure coefficient ( $0 \leq h \leq 1$ )
gs	Saturated unit weight (force\volume)
gm	Moist unit weight (force\volume)

Developing a static analysis, we specified the a, dn and IA values as 0, neglecting the seismic activity. The model did not perform the analysis on slopes with a gradient lower than the minimum slope value considered. This was done to prevent the calculation of extremely high Factors of Safety for shallow slopes. The z\_err factor depends on the DEM resolution; our value of 10 was adapted from literature as shown in following table:

Physical parameters (a)		
<b>Gw (Pa)</b>	<b>min_Slope (°)</b>	<b>z_err</b>
9810.0	5	10

Line 14, “soil”, contains the name of the input and an integer indicating the number of units contained in the lithological map. Our case of study presented 7 different units, therefore 7 groups of numbers, even though we only had 5 different lithologies (the map presented 7 distinct areas, the 5 lithologies are non-continuous due to the tectonic effects).

soils 7

phi normal 58 4.19 0  
cs normal 906 373.41 0  
d uniform 10 20 0  
h uniform 0.1 0.5 0  
gs normal 26701 2894.62 0  
gm normal 24826 2920.47 0

phi normal 48 3.08 0  
cs normal 381 65.20 0  
d uniform 2 10 0  
h uniform 0.1 0.5 0  
gs normal 26456 382.06 0  
gm normal 25456 382.06 0

phi normal 40 0. 0  
cs normal 55 40.71 0  
d uniform 10 20 0  
h uniform 0.1 0.5 0  
gs normal 22530 1950.71 0  
gm normal 20655 1978.88 0

phi normal 48 3.08 0  
cs normal 381 65.20 0  
d uniform 2 10 0  
h uniform 0.1 0.5 0  
gs normal 26456 382.06 0  
gm normal 25456 382.06 0

phi normal 61 3.40 0  
cs normal 1256 488.17 0  
d uniform 10 15 0  
h uniform 0.1 0.5 0  
gs normal 27584 547.59 0  
gm normal 26584 547.59 0

phi normal 40 0. 0  
cs normal 55 40.71 0  
d uniform 10 20 0  
h uniform 0.1 0.5 0  
gs normal 22530 1950.71 0  
gm normal 20655 1978.88 0

phi normal 43 5.16 0  
cs normal 354 104.53 0  
d uniform 10 20 0  
h uniform 0.1 0.5 0  
gs normal 27200 1927.44 0  
gm normal 25450 1992.31 0

Each line consisted of a variable's name abbreviation (for example "phi" for friction) followed by the name of the distribution type used:

- none: single value, constant;
- normal: two values, mean and standard deviation;

- empirical: two values, mean and standard deviation;
- uniform: two values, a minimum and a maximum value, has been used for the soil thickness and the water content parameters;
- triangular: three values, minimum, peak and maximum value;
- extreme: two values, location and scale parameters;
- beta\_pert: three values, a pessimistic, a most likely and an optimistic parameter.

There were six possible variables: friction, cohesion, layer thickness, water content, and dry and wet unit weight (table.13). Each variable includes three values, depending on the distribution type used. The normal and uniform distribution were used resulting in three values: average or maximum, standard deviation or minimum, and a dummy value of 0. The friction and cohesion values were determined after the field survey on rocks and soils, as well as the average layer thickness and water content. The layer thickness and the water content were defined using a uniform distribution, considering it constant for each lithology. We assigned an average maximum depth value of 20 m and a minimum average depth value of 10 m. The soil moisture has been assumed as between 10% and 50%, so  $h$  is equal to minimum 0.1 and maximum 0.5.

The unit weight of the soils, shown below, were determined from literature (E. Emir, A. Konuk and G. Dalgolu, (2011). Strength enhancement of Eskisehir tuff ashlar in Turkey and L.I. González de Vallejo, T. Hijazo, (2007). Geomechanical characterization of volcanic materials in Tenerife) and confirmed through inverse operations starting from the parameters evaluated in the field (see table 1 and table 2 for more details).

Unit weights of the lithologies					
Moist unit weight kN/m <sup>3</sup>	<b>Middle Jurassic</b>	<b>Upper Jurassic Rocks</b>	<b>Upper Jurassic Soils</b>	<b>Cretaceous</b>	<b>Neogene</b>
<b>average</b>	26.5838	24.8263	20.6550	25.4500	25.4563
<b>st.dev</b>	0.5476	2.9205	1.9789	1.9923	0.3821
<b>min</b>	26.01	20.01	18.54	22.55	25.01
<b>max</b>	27.5	28.27	24.03	28.44	26.22
Saturated Unit weight kN/m <sup>3</sup>	<b>Middle Jurassic</b>	<b>Upper Jurassic rocks</b>	<b>Upper Jurassic soils</b>	<b>Cretaceous</b>	<b>Neogene</b>
<b>average</b>	27.5838	26.7013	22.5300	27.200	26.4563
<b>st.dev</b>	0.5476	2.8946	1.9507	1.9274	0.3821
<b>min</b>	27.01	22.01	20.54	24.55	26.01
<b>max</b>	28.5	30.27	26.03	30.44	27.22

Following the last lithological unit, the forest coverage is described through 2 variables: root strength (cr) and tree surcharge (q), assumed as constant numbers throughout the area according to the literature. We choose the two values following C. Denning, U.S. Department of agriculture- The Slope Stability Reference guide for National Forests in the United States, (par. 4F, page 543 to 549) VOL2, 4F and analyzing the vegetation coverage of the area: cr = 2394 Pa and q = 239 Pa. The area is characterized by young and shallow vegetation, with roots that do not reach the deeper layers. It is important to keep the parameter units consistent because the model can produce an error by mixing them. The values used in the model are listed in the following table:

a) Physical parameters required for PISA-m (average±standard deviation)					
<b>Neogene</b>	<b>Cretaceous</b>	<b>Upper Jurassic soils</b>	<b>Upper Jurassic rocks</b>	<b>Middle Jurassic</b>	<b>Parameters</b>
48 (±3)	43 (±5)	30 (±)	58 (±4)	61 (±3)	<b>Friction Angle (°)</b>

380 ( $\pm 65$ )	350 ( $\pm 100$ )	63 ( $\pm 44$ )	910 ( $\pm 370$ )	1260 ( $\pm 490$ )	<b>Cohesive Strength (kPa)</b>
26.5 ( $\pm 0.4$ )	27.2 ( $\pm 2$ )	22.5 ( $\pm 2$ )	26.7 ( $\pm 3$ )	27.6 ( $\pm 0.5$ )	<b>Saturated Unit Weight (<math>\text{kN}\text{m}^3</math>)</b>
25.5 ( $\pm 0.4$ )	25.5 ( $\pm 2$ )	20.7 ( $\pm 2$ )	24.8 ( $\pm 3$ )	26.6 ( $\pm 0.5$ )	<b>Moist Unit Weight (<math>\text{kN}\text{m}^3</math>)</b>

The PISA-m output file was an ASCII, results.asc file. The result.asc file was converted to a raster file using ArcMap. This was done to save time in processing the analysis, and because for any time the model runs it will overwrite the original result.asc. The results show that the Factor of Safety is low in the area considered.

### 3.4.5 Results

After processing the data, the susceptibility map of the area observable was obtained in Figure 49. The Factor of Safety values obtained were initially classified as unique values on the map. These values were reclassified following this strategy: the area where FS is equal to 0 has been assumed to be an already failed area while FS between 0 and 1 and between 1 and 2 represent a high vulnerability and a medium vulnerability area, respectively. The highest FS values, greater than 2, were considered stable. The Factor of Safety distributions reflect the geometry of the lithological map to highlight the geological limits between the different sediments. The area shown in Figure 49 as already failed is the clay area occupied by Khoko. We evaluated how sensitive the model is to each parameter, modifying the cohesion, vegetation values, humidity and so on. The most inconsistent value noticed was the friction which was initially zero for the Jurassic soils. The variation of the susceptibility map is evident in the Jurassic area by increasing the phi value from 0 to 10, then from 10 to 30. The zones clearly become more stable as the FS increase locally.

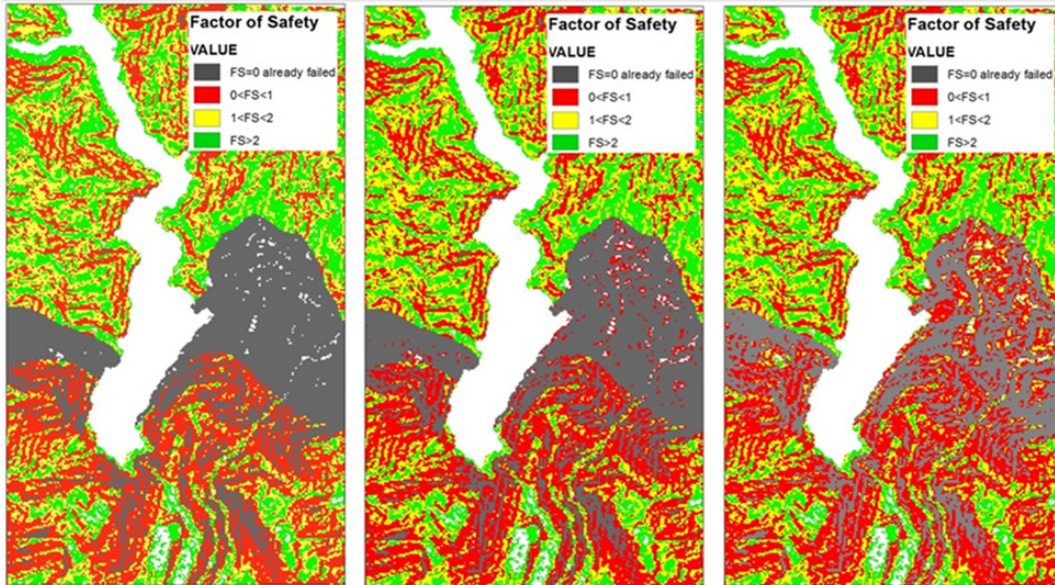


Figure 49: PISA-m results. Spatial distribution of the safety factor around the area for different values of friction ( $\Phi$ ). a)  $\Phi=0$  b)  $\Phi=10$  c)  $\Phi=30$

From the model results, all the Jurassic soils area had a Factor of Safety smaller than 1, which explains the existent situation: the zone has already failed. The values on the adjacent area are low as well. The tests variations show that the FS increased with the increasing of the friction and cohesion but did not change with the vegetation or unit weight values.

### 3.5 2D FEM-SSR Modeling

The purpose of this study was to conduct a current state stability analysis carried out with FEM-SSR methods to investigate, as much as possible, the associated deformation and breakdown mechanisms. There are several kinds of data necessary to perform this analysis:

- Topography and Geological section

The analysis started from a geological cross section of the area of the Khoko landslide drawn in the framework of the project SPS. The cross-section trace was SSW-NNE trending and 2900 m long. It went from the bottom of the lake to the area immediately above the principal road, where the team identified the main scarp of the landslide. There was a strong uncertainty about the stratigraphy, which is why different methods of analysis were used in hypnotizing presence or absence of a weathered bedrock and its thickness. Borehole data and surveys in the field were used to conclude the stratigraphy.

- Mechanical properties

The mechanical properties used in the current analysis were determined after testing the model with different values. The data used was from an average between our field measurements and ones from a report of the Center Geodynamic Studies LLC "CGI" of Moscow "Implementation of a complex engineering-geological survey of the left bank of the landslide in the reservoir area of arch dam LLC and slope stability analysis".

- Groundwater

We decided to use the Piezo Line groundwater method by setting the lake level to be 510m (Figure 50) in the first test and 430m in a second test following the data from the report of the Center Geodynamic Studies LLC "CGI" of Moscow. On the slope, we set up the piezometric line tangent to the surface because once in the field we noticed several springs all over the area.

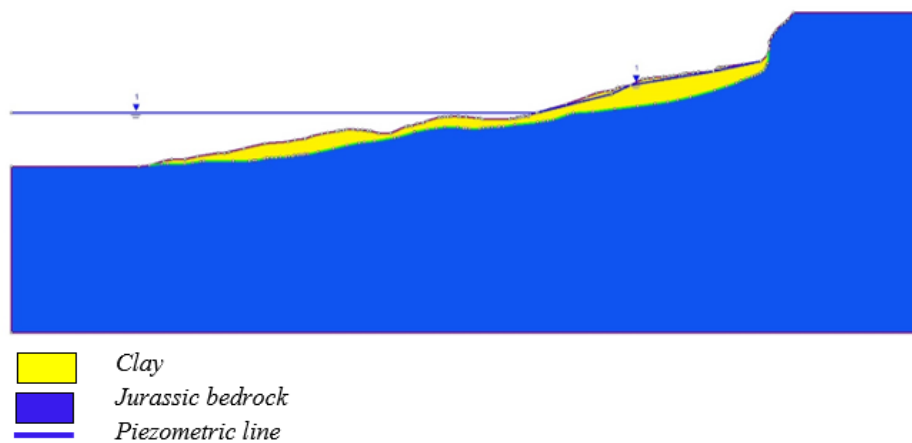


Figure 50: 2D section of the slope on Phase2 (Total Head 510m)

The Finite Element Method (FEM) works on a stress-strain relationship and performs a numerical analysis of each elementary cell by studying the mechanics of several interconnected cells and the evolution of the stress conditions. In a Phase2 FEM model, the strength parameters of a slope were reduced by different values of a strength reduction factor (SRF) until the model became unstable, this way a finite element slope stability analysis is performed. As explained in the Rocscience Phase2 tutorials, the option that allows performing an FEM slope stability analysis in Phase2 is the shear strength reduction (SSR). The 2D geological section available was digitized and recreated on Rocscience Phase2 9.002, available at UNIMIB. The three lithologies present on the model were the intact Jurassic bedrock, the weathered Jurassic bedrock, and the Quaternary clays (see chapter 2.4.2 about the geology of Enguri Dam). The Quaternary clays, specifically, were the most recently collapsed, loose, and reshuffled materials deriving from the most superficial Jurassic deposits.

To take into account the different uncertainties encountered in the definition of the model stratigraphy, material properties, and initial conditions, we performed different models corresponding to different scenarios, namely:



- MODEL.1: Jurassic assumed as intact bedrock at the bottom, clay at the top, complete saturation
- MODEL.2: Jurassic assumed as intact bedrock at the bottom, clay at the top, just clay saturation (Figure 51, 52, 53, 54)
- MODEL.3: Jurassic assumed as weathered bedrock at the bottom, clay at the top, complete saturation
- MODEL.4: Jurassic assumed as weathered bedrock at the bottom, clay at the top, just clay saturation

This model was obtained using the Plane Strain Analysis Type. The units of the physical parameters were meters, seconds, degrees, kN, and kPa. The slope stability analysis using finite elements started from an initial estimate of SRF as 1. To obtain a better overview, the software also performed a groundwater analysis using the Piezometric Lines method, assuming a pore fluid unit weight of 9.81 kN/m<sup>3</sup> and adding a ponded distributed load oriented normal to the boundaries (Total Head = 510 m). For each scenario, the piezometric line was adjacent to the surface due to the appearance of several springs around the area of the main road and on the lakeshore and the fact that water floats on the surface of almost all the boreholes. The total stress ratio is 0.4 due to the imposed field stress, Gravity, and the actual ground surface. The model needed a finite mesh element to compute properly. The mesh type used was a uniform 8 m nominal element length for the clays and a graded 75 m nominal element length for the Jurassic with six-node triangles. The initial element loading of the material properties was set as “field stress & body force”, where the elastic type was “Isotropic” and the failure criterion used was Mohr-Coulomb. The other physical parameters were set as default for both lithologies:

	$\Phi$ (°)	c (kPa)	Y (kN/m <sup>2</sup> )	E (kPa)	PTS (kPa)	RTS (kPa)	v
CLAY	20	50	19.55	100,000	20	0	0.3
WB	32	100	22	10,000,000	50	0	0.3
IB	35	200	25	10,000,000	100	0	0.3

$\Phi$ : friction

c: cohesion

Y: unit weight of soil

E: Young's modulus

PTS: Peak tensile strength

RTS: Residual tensile strength

v: Poisson's ratio

After running the four sceneries on Phase2 and analyzing the results, exploring the SRF values, the maximum shear plastic strain, the horizontal, vertical and total displacement, and the volumetric strain we opted to use model 2 for its most realistic output (Figure 51, 52, 53, 54). The Jurassic was assumed to be Intact Bedrock at the bottom, and clay at the top with only clay saturation. This model gives an SRF value higher than the others, but still too low (0.7), and gives two sliding curved surfaces inside the clay layer. The results show that the instability of the scarp area does not influence model 2 as much the others: models 1, 3, and 4 (see tables). The calculations developed a Rankine wedge with high values of shear plastic strain that influence the entire system. Since we were interested in evaluating (see the chapter about the geology of Enguri Dam) the downward movement of the slope and the shape of the detachment surfaces we choose model 2. The results obtained from the models are consistent with the situation. At the site, in fact, there was evidence of an instability: loose materials such as curved tree trunks, breakages on road lanes under the landslide scarp, and fissures all over the top.

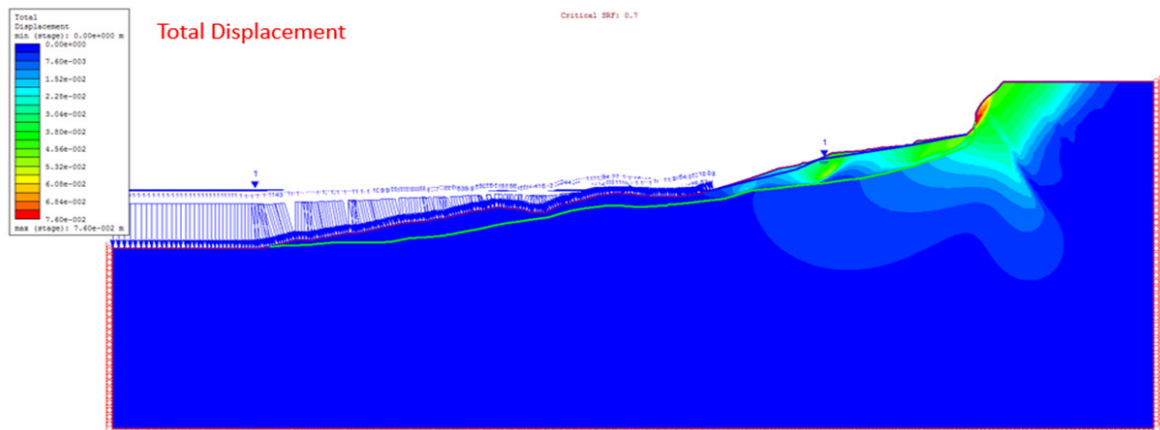
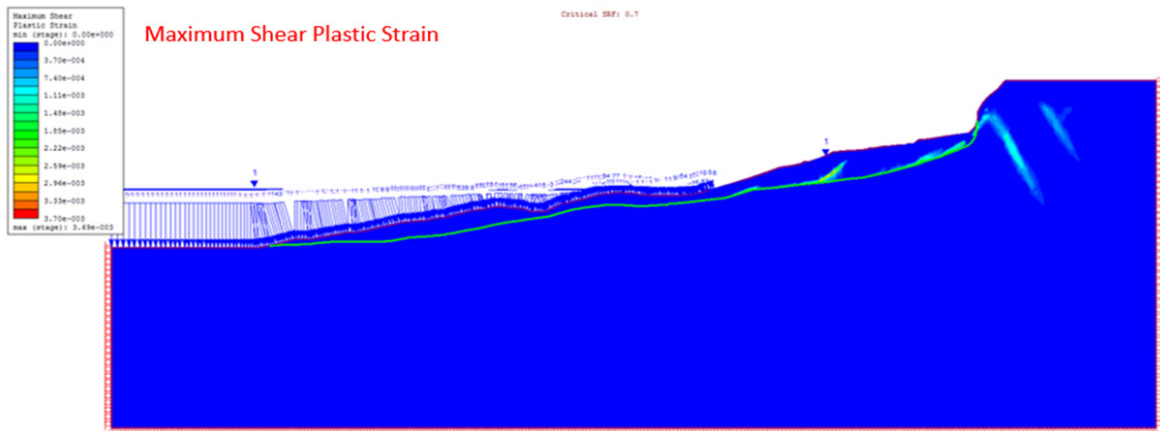


Figure 51: Maximum Shear Plastic Strain MODEL2

Figure 52: Total Displacement MODEL2

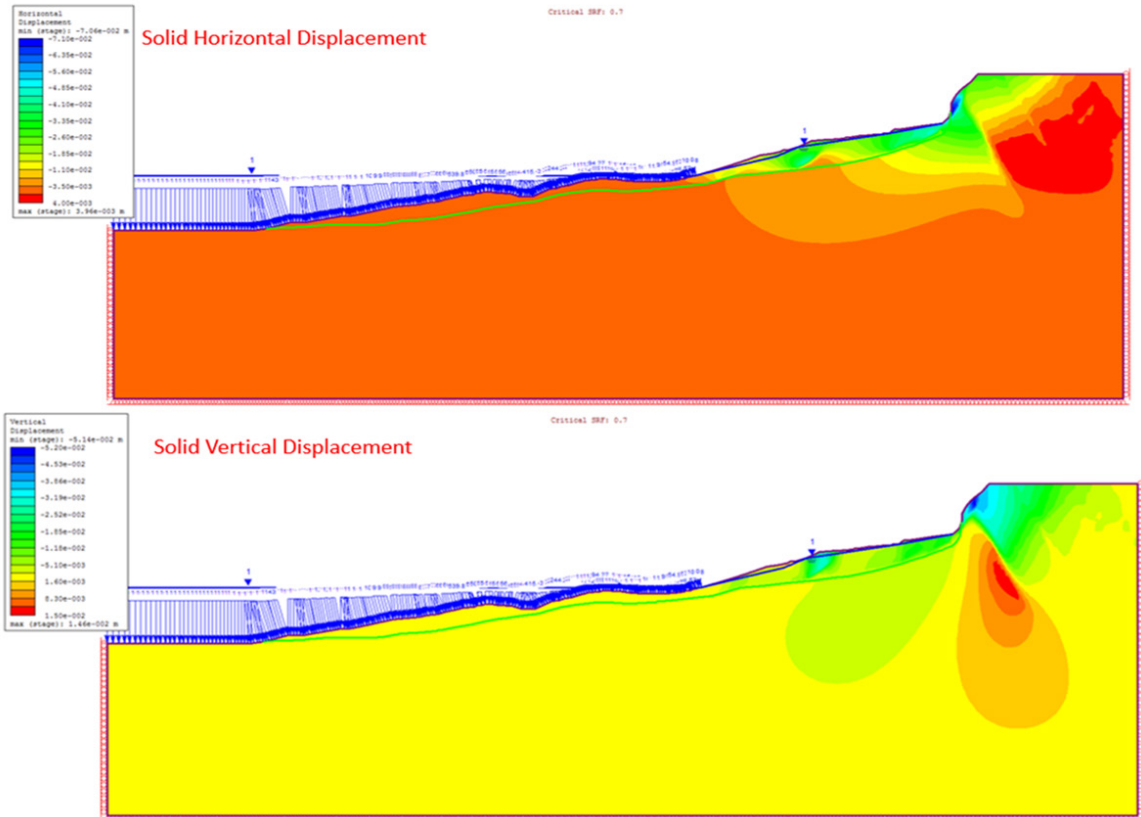


Figure 53: Solid Horizontal Displacement MODEL2

Figure 54: Solid Vertical Displacement MODEL2

Operating with some variations, we created MODEL2.A (Figure 55) and decided to add a new material boundary at the top to isolate the area of the landslide scarp. It was assigned highly strong properties in order to prevent localized instability in this sector that would affect the calculation of an SRF value representative of the behavior of the landslide. Because of this, the SRF increased from 0.7 to 1.08, a value more consistent with field evidence and the model gave more information about the slope instead of the top which is now stable. To obtain a better result, we created an additional model, the MODEL2.B (Figure 66), where an intermediate layer of weathered bedrock about 60m thick was added between the clays and the intact bedrock. This allowed us to test the effects of hypotheses and uncertainties on the geometry of a weathered bedrock layer, which remained unclear after a detailed analysis of available borehole logs.

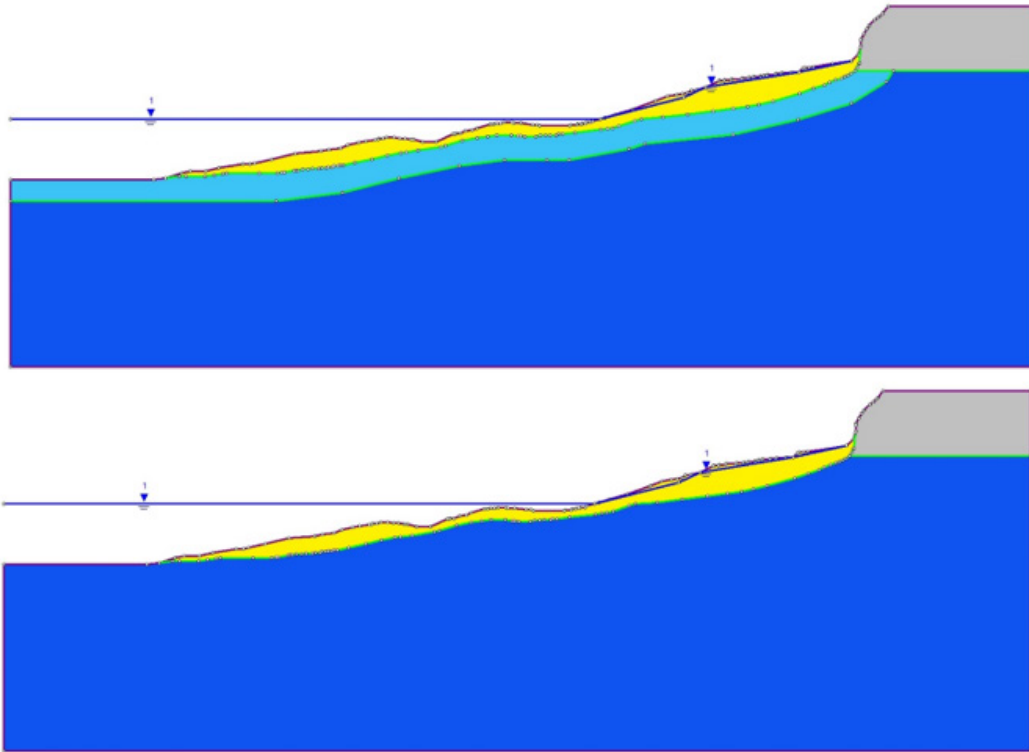


Figure 55: Phase2 MODEL2.A

Figure 56: Phase2 MODEL2.B

	$\Phi$ (°)	c (kPa)	Y (kN/m <sup>2</sup> )	E (kPa)	PTS (kPa)	RTS (kPa)	v
<b>CLAY</b>	20	50	19.55	100,000	20	0	0.3
<b>WB</b>	32	100	22	10,000,000	50	0	0.3
<b>IB</b>	35	200	25	10,000,000	100	0	0.3
<b>STABLE</b>	50	500	27	10,000,000	100	0	0.3

**SRF MODEL2.A= 1.08**

**SRF MODEL2.B= 1.07**

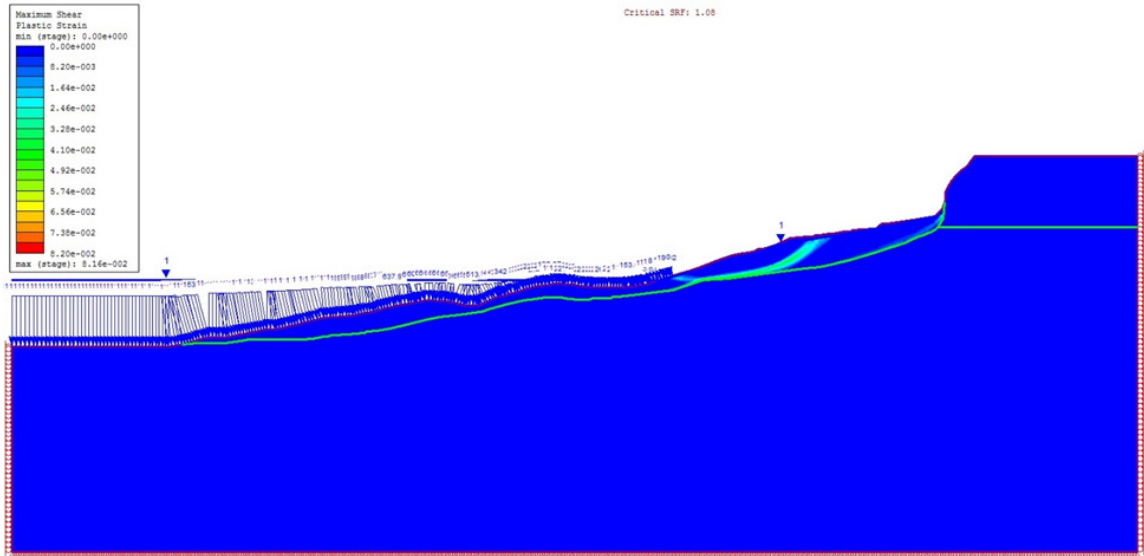


Figure 57: Shear Plastic Strength MODEL 2.A

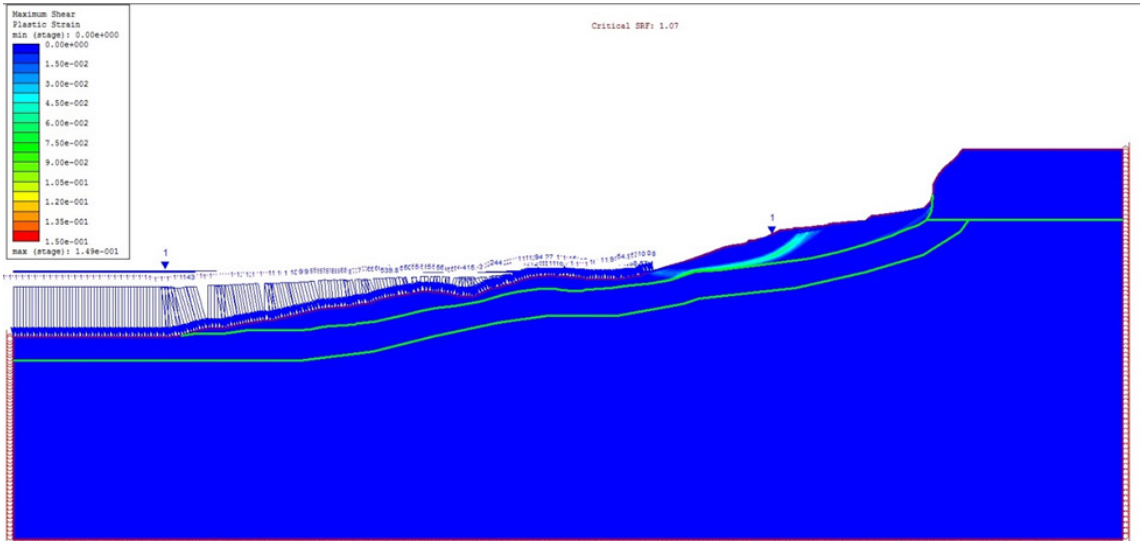


Figure 58: Shear Plastic Strength MODEL 2.B

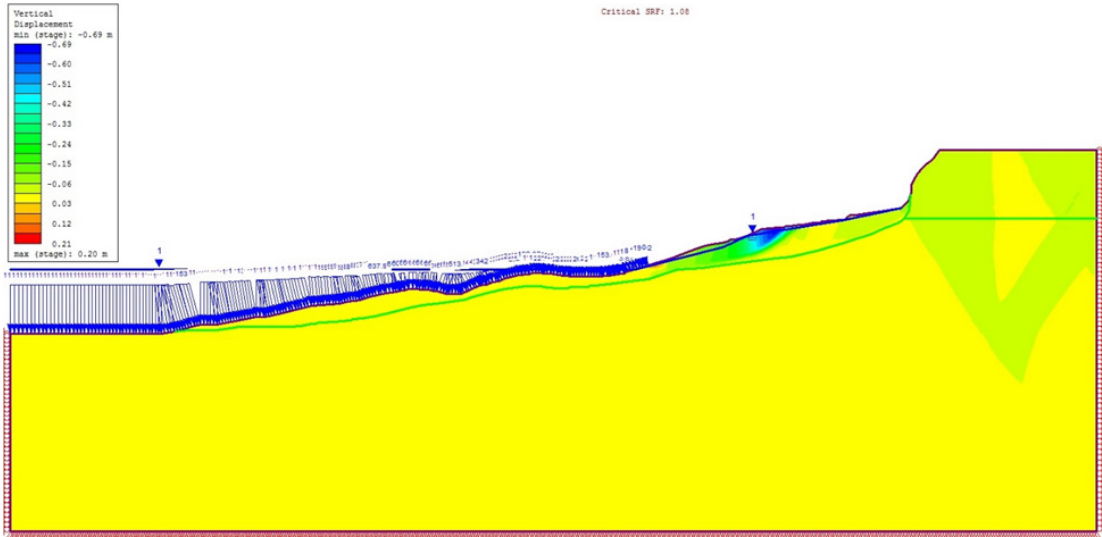


Figure 59: Solid Vertical Displacement MODEL 2.A

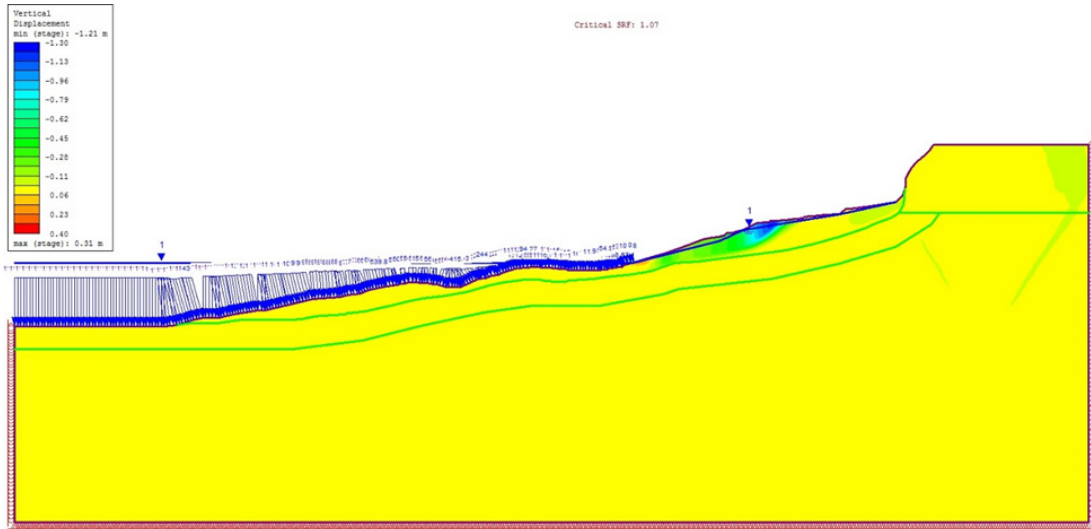


Figure 60: Solid Vertical Displacement MODEL 2.B

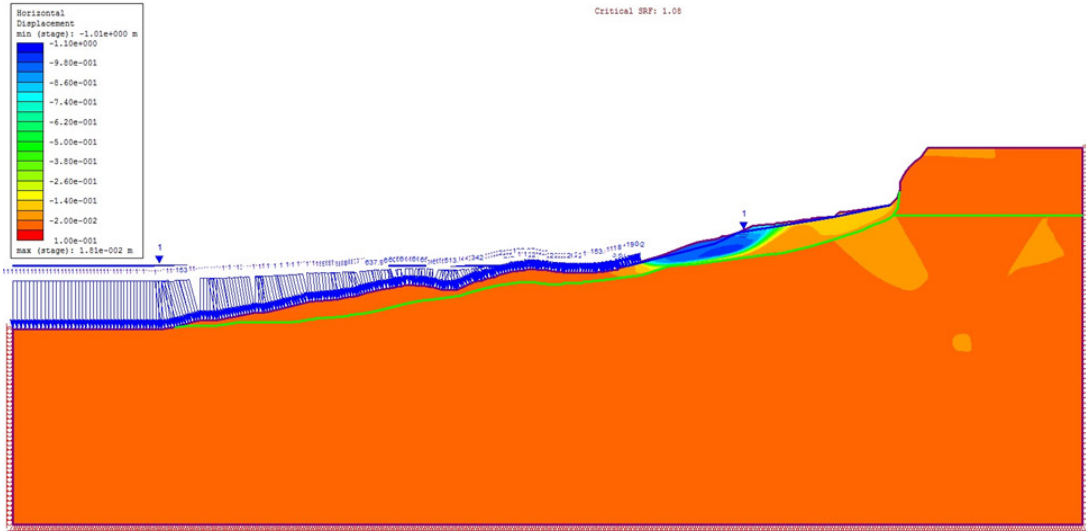


Figure 61: Solid Horizontal Displacement MODEL 2.A

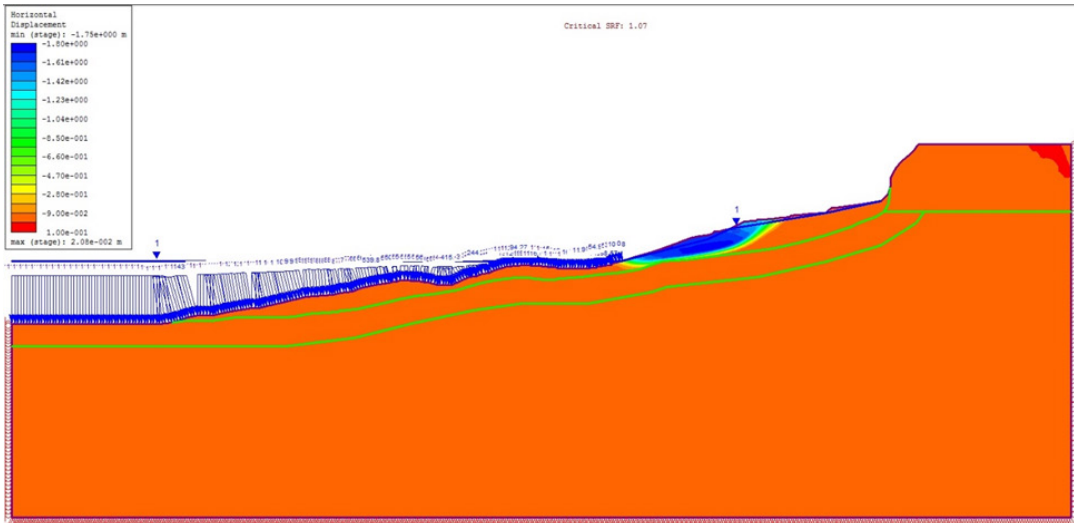


Figure 62: Solid Horizontal Displacement MODEL 2.B

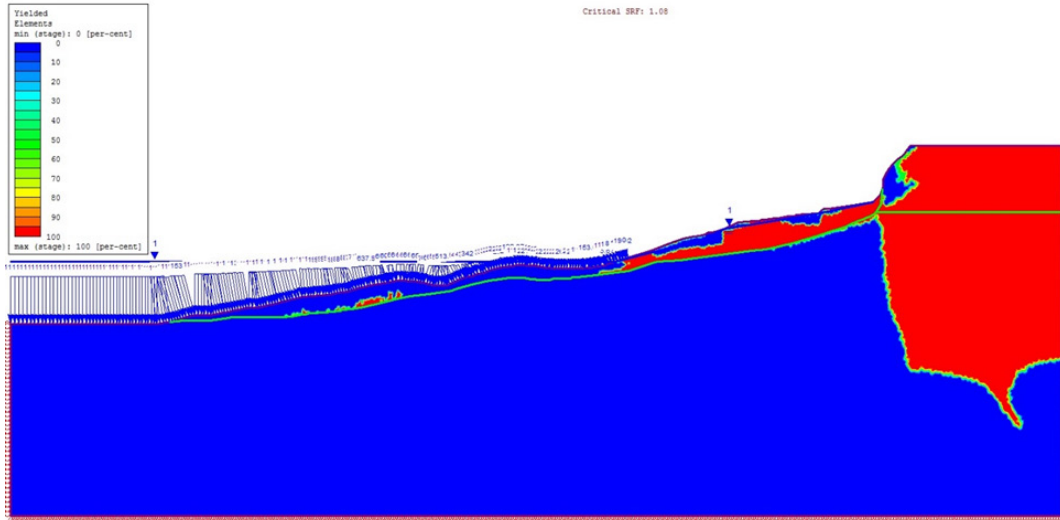


Figure 63: Yielded Elements MODEL 2.A

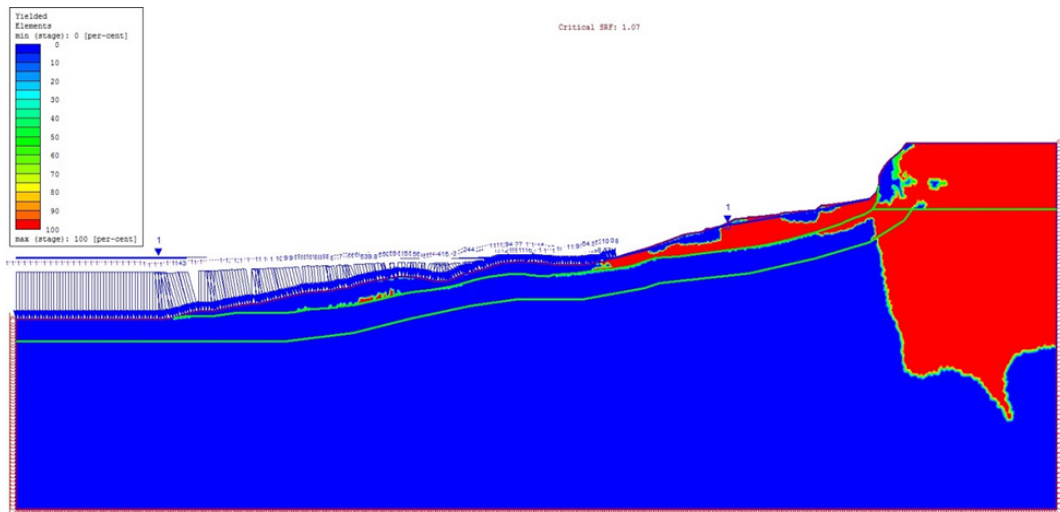


Figure 64: Yielded Elements MODEL 2.B

The results obtained from the two models were very similar. It was concluded that the weathered layer does not seem to be influencing the stability of the area so a homogeneous Jurassic bedrock, with no distinction between the weathered and intact parts was considered as the final model, the 2.A. At this point, we started testing on the MODEL2.A, creating a further model in Rocscience Phase2, decreasing the Piezometric Line Total Head from 510m to 430m. This new model (MODEL 2.A.430) showed that the situation does not change much: the SRF decreased from 1.08 to 1.01. The only difference was that the detachment surface died against the lake level in the MODEL2.A, and in MODEL.2.A.430 follows the lithological limit as gradually thinning. Similarly, the area between the slipping surface and the scarp deforms more in MODEL2.A compared to MODEL2.A.430.



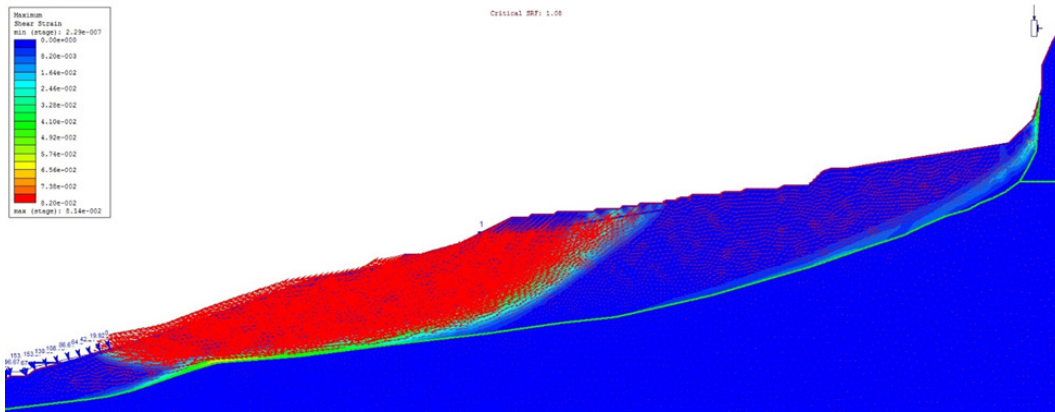


Figure 65: Maximum Shear Plastic Strain and deformation vectors MODEL 2.A

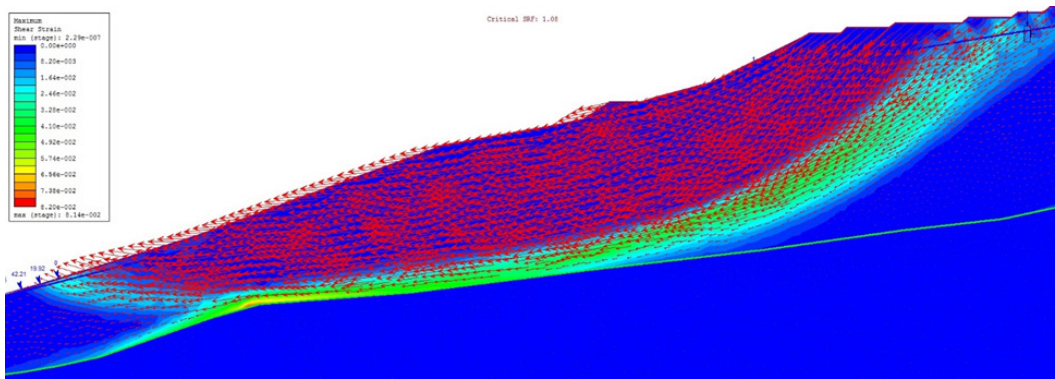


Figure 66: Maximum Shear Plastic Strain and deformation vectors zoom MODEL 2.A

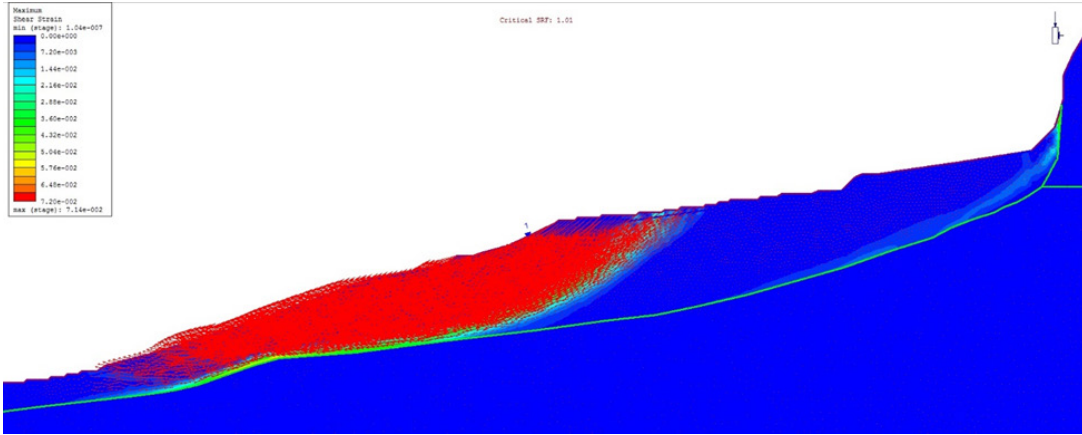


Figure 67: Maximum Shear Plastic Strain and deformation vectors MODEL2.A.430

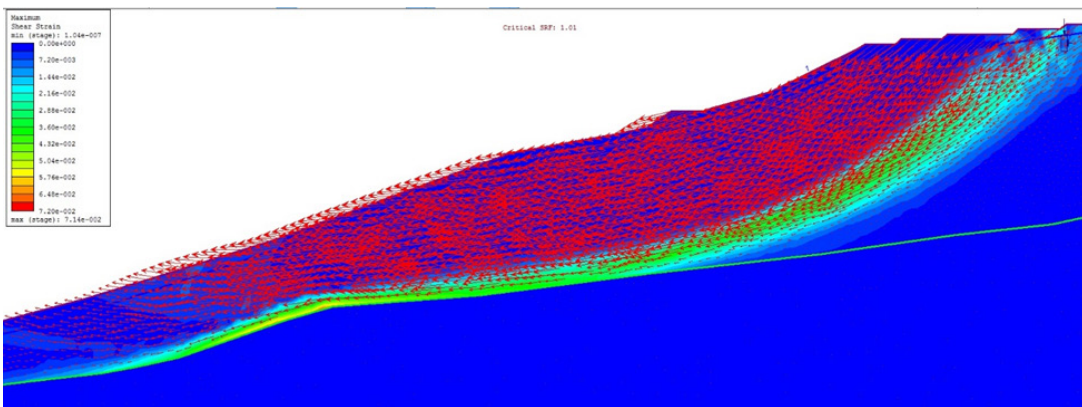


Figure 68: Maximum Shear Plastic Strain and deformation vectors zoom MODEL2.A.430

Furthermore, we used Slide to perform a Limit Equilibrium Probabilistic slope stability analysis and compare the Safety factor (FS) with the previous SRF. The LEM analysis, even though it is less reliable than the FEM, allowed us to further analyze the detachment surface position and compare the factor of safety values. Theoretically, the Critical SRF in Phase2 corresponded to the FS in Slide. A Safety Factor equal to 1 meant the slope was in a state of limited equilibrium. A reduction in shear strength resulted in failure of the slope. In this case  $SRF=1.06$  and  $FS=1.141$ .

Figures 69 and 70 show the minimum surfaces at slip center grid points in the Janbu and simplifies specific case for the MODEL 2.A. with the piezometric line at 510 m and 430 m. There is a difference of 0.066 between the two FS. As the models show, the results are consistent with the evidence of an instability in the field. The evident detachment surfaces appear only in the Quaternary layer in each situation and, in the field, correspond to the areas with the most pervasive surface of deep fracturing. While close to the lakeshore, the slope appeared to be the stable toe of the earth flow, up slope the most unstable portions are the area under the landslide scarp and the central one. The landslide seemed to be a nested rotational type landslide an earth flow. An interesting result

regarding the lake was that the lake generates a push that makes the foot of the slope stable, so the movement of sediments seemed to stop at the lake level and the structure appear stable. The most vulnerable portion appeared in the middle, evident in both the models (phase and slide).

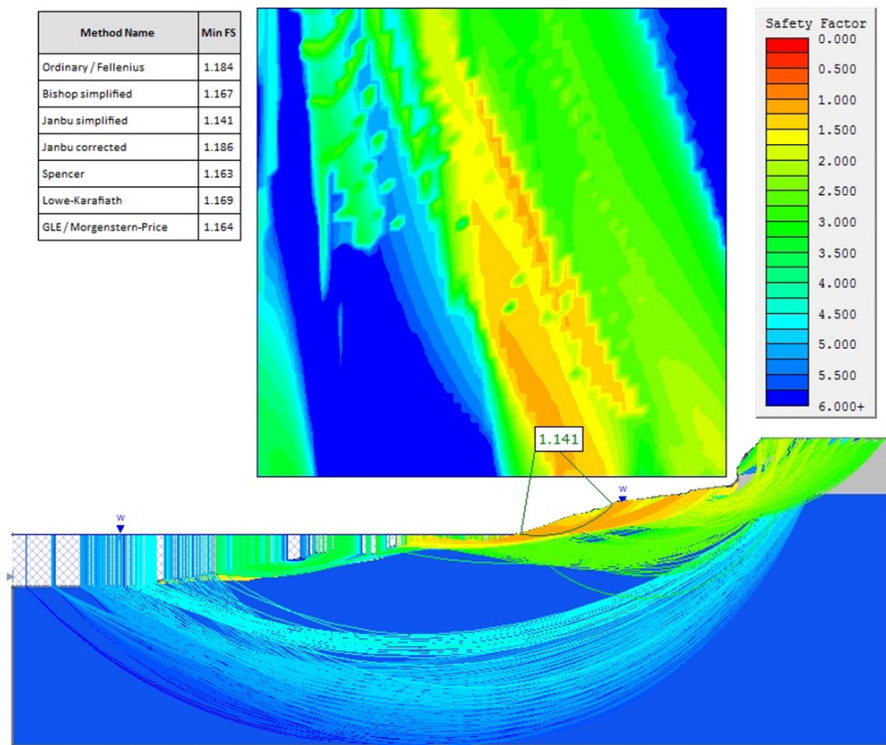


Figure 69: Slide MODEL2.A (FS for Janbu Simplified)

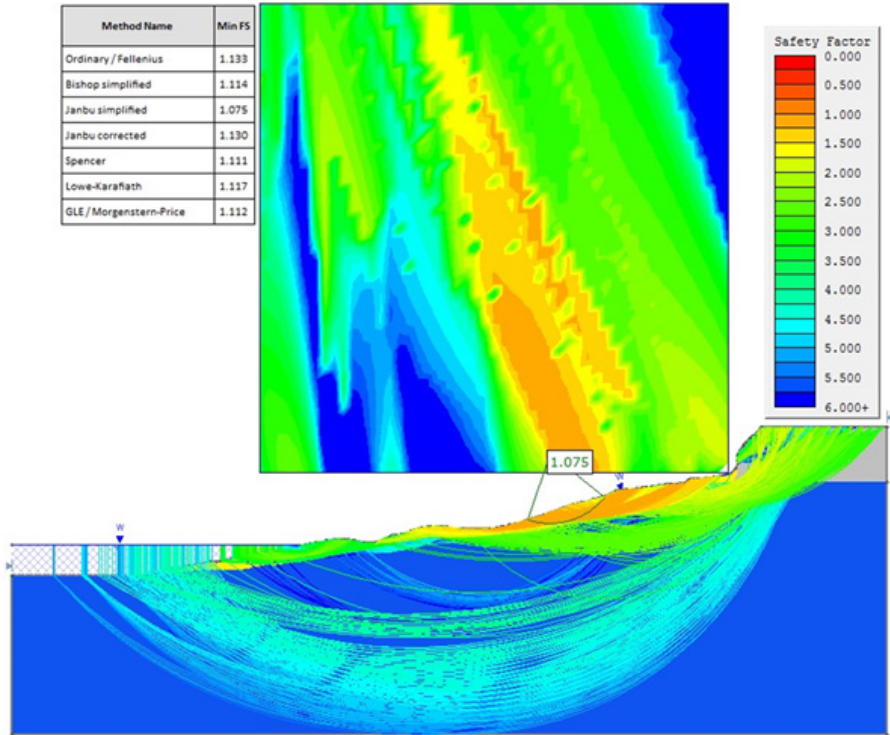


Figure 70: Slide MODEL2.A.430 (FS for Janbu Simplified)

## 4 Results

From the PISA-m results it was concluded that the Jurassic soils area had a Factor of Safety smaller than 1 and the adjacent area had a much lower FS that increased with friction and cohesion values but didn't change with the vegetation or unit weight values. The Phase2 and Slide models confirmed that the most unstable areas of the slope were the ones under the landslide scarp of Khoko and the ones downslope of the central part. The unstable areas on the models corresponded to the visible unstable, fractured or deformed areas in the field. This is evidenced by curved tree trunks, swelling of the surfaces, fissures at the top of the landslide, fractures on the scarp area and strong subsidence of the main road. From the results, the lake seemed to give a strong push that stabilized the slope holding it with a counterforce that created a stable area. Finally, it would be appropriate to implement specific mitigation techniques for each lithologic unit and type of gravitational movement to stabilize the different areas. An example would be imposing passive defense works such as rock fall barriers in areas characterized by limestones outcrops, or deep drainage systems for the more clay-like slopes.

## 5 Reference List and Copyright documentation

- S. Adamia, V. Alania, A. Chabukiani, Z. Kutelia, N. Sadradze, (2011). Great Caucasus (Cavcasioni): A Long-lived North-Tethyan Back-Arc Basin
- S. Adamia, A. Chabukiani, T. Chkhotua, N. Sadradze, D. Zakaraia, G. Zakariadze, (2010). Geology of The Caucasus And Adjacent Areas: 1:2 500 000 SCALE GEOLOGICAL MAP
- S. Adamia, G. Zakariadza, T. Chikhotua, N. Sadrazei, N. Tsereteli, A. Chabukiani & A. Gventsadze, (2011). Geology of the Caucasus: A Review
- F. Agliardi, G. Crosta, A. Zanchi, (2001). Structural constraints on deep-seated slope deformation kinematics
- J. Blatter and H. Ingram (2001). Reflections on water: new approaches to transboundary conflicts and cooperation. MIT Press. pp. 221–2
- M. Bordoni, C.Meisina, R. Valentino, N. Luc, M. Bittelli, S. Chersich, (2015). Hydrological factors affecting rainfall-induced shallow landslides: From the field monitoring to a simplified slope stability analysis
- C. Chalkias, M. Ferentinou and C. Polykretis, (2014). GIS-Based Landslide Susceptibility Mapping on the Peloponnese Peninsula, Greece
- T. Chelidze, Z. Javakhishvili, O. Varazanashvili, M. Elashvili, Y. Kolesnikov, T. Godoladze, N. Butikashvili, E. Ghlonti. Seismic hazard assessment of Georgia (probabilistic approach)
- T. Chelidze, T. Matcharashvili, V. Abashidze, M. Kalabegishvili, N. Zhukova, (2013). Real time monitoring for analysis of dam stability: potential of nonlinear elasticity and nonlinear dynamics approaches
- R.A. Cole. Map-based Probabilistic Infinite Slope Analysis of the Stephens Creek Watershed, Portland, Oregon
- J. Corominas, C. van Westen, P. Frattini, L. Cascini, J.P. Malet, S. Fotopoulou, F. Catani, M. Van Den Eeckhaut, O. Mavrouli, F. Agliardi, K. Pitilakis, M. G. Winter, M. Pastor, S. Ferlisi, V. Tofani, J. Herv's, J. T. Smith, (2013). Recommendations for the quantitative analysis of landslide risk
- G.B. Crosta, F. Agliardi, (2002). A methodology for physically based rockfall hazard assessment

D.M. Cruden, D.J. Varnes, (1996). Landslides: investigation and mitigation. Chapter 3: Landslides type and processes, Transportation research board, National Academy of Sciences.

C. Denning. U.S. Department of agriculture- The Slope Stability Reference guide for National Forests in the United States. (Par. 4F, page 543 to 549) VOL2, 4F

A.Di Iorio, B. Laserre, G.S. Scippa and D.Chiatante, (2004). Root System Architecture of Quercus pubescens Trees Growing on Different Sloping Conditions

E. Emir, A. Konuk and G. Dalog˘lu, (2011). Strength enhancement of Eskisehir tuff ashlar in Turkey

ESRI website tutorials, International supplier of Geographic Information System (GIS) software, web GIS and geodatabase management applications

P. Fisher, (1998). Improved Modeling of Elevation Error with Geostatistics

P. Frattini, G. Crosta, A. Carrara, (2009). Techniques for evaluating the performance of landslide susceptibility models

P. Frattini, G. Crosta, A. Carrara, F. Agliardi, (2007). Assessment of rockfall susceptibility by integrating statistical and physically- based approaches

J. Garrett. Gis-based landslide susceptibility analysis of southwestern Colorado Springs, El Paso County, Colorado

L.I. González de Vallejo, T. Hijazo, (2007). Geomechanical characterization of volcanic materials in Tenerife

T. Gavtadze, K. Mikadze, Z. Chkhaidze, (2010). Biostratigraphy and palaeoenvironment of the upper cretaceous flysch sediments of the mestia-tianeti zone of the Greater Caucasus fold system

W.C. Haneberg. "PISA-m Map-Based Probabilistic Infinite Slope Analysis" Version 1.0.1, User Manual Updated March 2007

K.W. Holmesa, O.A. Chadwicka, P.C. Kyriakidisb. Error in a USGS 30-meter digital elevation model and its impact on terrain modeling

R.W. Jibson- Predicting Earthquakes. Induced Landslide displacements using Nwemark's Sliding Block Analysis

U. Kamp, B.J. Growley, G.A. Khattak, L. A. Owen, (2008). GIS-based landslide susceptibility mapping for the 2005 Kashmir earthquake region

- V. G. Kazmin, (2005). Tectonic Evolution of the Caucasus and Fore-Caucasus in the Late Paleozoic
- K. K. Kwang, M. Prezzi, R. Salgado, (2006). Interpretation of Cone Penetration Tests in Cohesive Soils
- A.Kwan Leung, A. Garg, C. WangWai Ng, (2015). Effects of plant roots on soil-water retention and induced suction in vegetated soil
- G. Kordzakhia, L. Shengelia, G. Tvauri, M. Dzadzamia. Research of Devdoraki Glacier Based on Satellite Remote Sensing Data and Devdoraki Glacier Falls in Historical Context
- H.A. Loáiciga, (2015). Groundwater and earthquakes: Screening analysis for slope stability
- L. Lu, Z.J.Wang, M.L. Song, K. Arai, (2015). Stability analysis of slopes with ground water during earthquakes
- L. I. Malyshev, K. I. Maksimov, P. S. Sokolovskii. On site investigations of seepage in the foundation of the Inguri dam during construction
- F. Mayringer, P.J. Treloar, Gerdes, F. Finger, D. Shengelia, (2011). New Age Data from The Dzirula Massif, Georgia: Implications for The Evolution Of The Caucasian Variscides
- T. Mumladze, A. M. Forte, E. S. Cowgill, C. C. Trexler, N. A. Niemi, M. B. Yıkılmaz, L. H. Kellogg, (2014). Subducted, detached, and torn slabs beneath the Greater Caucasus
- MER. Advisory Review of the Environmental and Social Impact Assessment of the Khudoni Hydropower Project
- A.Nandi, A. Shakoor, (2009). A GIS-based landslide susceptibility evaluation using bivariate and multivariate statistical analyses
- NATO Project G4934, Science for Peace and Security Programme. Dropbox group sharing “Security against geohazards at the major Enguri hydroelectric scheme in Georgia”
- E. Nikolaeva, T.R. Walter, M. Shirzaei and J. Zschau, (2014). Landslide observation and volume estimation in central Georgia based on L-band InSAR
- Pacific Watershed Associates Report No. 08076901. Slope Stability Modeling and Landslide Hazard in Freshwater Creek and Ryan Slough, Humboldt County, California



- H. R. Pourghasemi, B. Pradhan, C. Gokceoglu and K. D. Moezzi. Landslide Susceptibility Mapping Using a Spatial Multi Criteria Evaluation Model at Haraz Watershed, Iran
- J. Rusnak, C. Mark. Using the Point Load Test to determine the Uniaxial Compressive Strength of coal measure rock.
- S. Sarkar, D.P. Kanungo, A.K. Patra and Pushendra Kumar. GIS Based Landslide Susceptibility Mapping, A Case Study in Indian Himalaya
- A.I. Savich, M.M. Iliin, M.G. Ezersky, N.I. Kalinin, (1983). Long-term geophysical observations on the inguri dam rock foundation (Bulletin of the International Association of Engineering Geology)
- K.M. Schmidt, J.J. Roering, J.D. Stock, W.E. Dietrich, D.R. Montgomery, and T. Schaub, (2001). The variability of root cohesion as an influence on shallow landslide susceptibility in the Oregon Coast Range
- O. Simpson Nyambane, S. Kinyua Mwea, (2011). Root tensile strength of 3 typical plant species and their contribution to soil shear strength; a case study: Sasumua Backslope, Nyandarua District, Kenya
- M. Sosson, R. Stephenson, Y. Sheremet, Y. Rolland, S. Adamia, R. Melkonian, T. Kangarli, T. Yegorova, A. Avagyan, G. Galoyan, T. Danelian, M. Hassig, M. Meijers, C. Muller, L. Sahakyan, N. Sadradze, V. Alania, O. Enukidze, J. Mosar, (2015). The eastern Black Sea-Caucasus region during the Cretaceous: New evidence to constrain its tectonic evolution
- A. Stinghen, M. Massironi, S. Furlani, G. Monegato, (2011). Evoluzione Tettonica E Geomorfologica Del Bacino Di Kartalini, Georgia
- L. Telesca, T. Matcharasvili, T. Chelidze and N. Zhukova, (2012). Relationship between seismicity and water level in the Enguri high dam area (Georgia) using the singular spectrum analysis
- B. Thiebes, R. Bell, T. Glade, S. Jäger, M. Anderson, L. Holcombe, (2013). A Web GIS decision-support system for slope stability based on limit-equilibrium modelling
- United States Agency for International Development, Deloitte Consulting- Hydropower investment promotion project (HIPP,) 2012
- USGS website. U.S. Geological Survey [www.usgs.gov/](http://www.usgs.gov/), United States Geological Survey. Scientific agency for natural sciences, including earth science and biology
- E. Weppner, J. Hoyt and W. Haneberg. Slope Stability Modeling and Landslide Hazard in Freshwater Creek and Ryan Slough Humboldt County, California

M. Wieland. Earthquake safety of concrete dams and seismic design criteria for major dam projects

A.Yassaghia, H.Salari-Radb and H. Kanani-Moghadam, (2004). Geomechanical evaluations of Karaj tuffs for rock tunneling in Tehran–Shomal Freeway, Iran

R. R. Ziemer. Pacific Southwest Forest and Range Experiment Station Forest Service, U.S. Dept. of Agric., 1700 Bayview Dr., Arcata, CA, USA. The role of vegetation in the stability of forested slopes.

COPYRIGHT:

<https://www.google.com/maps/?hl=it>

<https://earth.google.com/web/>

[https://en.wikipedia.org/wiki/Enguri\\_Dam](https://en.wikipedia.org/wiki/Enguri_Dam)

<http://www.enguriproject.unimib.it/>